



Article

Dynamic Heat Transfer Modelling and Thermal Performance Evaluation for Cadmium Telluride-Based Vacuum Photovoltaic Glazing

Changyu Qiu 1,* D, Hongxing Yang 2 and Kaijun Dong 1,*

- ¹ Guangzhou Institute of Energy Conversion, Chinese Academy of Sciences, Guangzhou 510640, China
- Department of Building Environment and Energy Engineering, The Hong Kong Polytechnic University, Hong Kong, China; hong-xing.yang@polyu.edu.hk
- * Correspondence: cy.qiu@connect.polyu.hk (C.Q.); dongkj@ms.giec.ac.cn (K.D.)

Abstract

Building-integrated photovoltaic (BIPV) windows present a viable path towards carbon neutrality in the building sector. However, conventional BIPV windows, such as semitransparent photovoltaic (STPV) glazings, still suffer from inadequate thermal insulation, which limits their effectiveness across different climate conditions. To address this issue, the cadmium telluride-based vacuum PV glazing has been developed to enhance the thermal performance of BIPV applications. To fully understand the complex thermal behaviour under real-world operational scenarios, this study introduces a one-dimensional transient heat transfer model that can efficiently capture the time-dependent thermal dynamics of this novel glazing system. Based on the numerical solutions using the explicit finite difference method (FDM), the temperature profile of the vacuum PV glazing can be obtained dynamically. Consequently, the heat gain of the semi-transparent vacuum PV glazing can be calculated under time-varying outdoor and indoor conditions. The validated heat transfer model was applied under four different scenarios, viz. summer daytime, summer nighttime, winter daytime, and winter nighttime, to provide a detailed analysis of the dynamic thermal behaviour, including the temperature variation and the energy flow. The dynamic thermal characteristics of the vacuum PV glazing calculated by the transient heat transfer model demonstrate its excellent thermal insulation and solar control capabilities. Moreover, the thermal performance of vacuum PV glazing was compared with a standard double-pane window under various weather conditions of a typical summer day and a typical winter day. The results indicate that the vacuum PV glazing can effectively minimise both heat gain and heat loss. The fluctuation of the inner surface temperature can be controlled within a limited range away from the set point of the indoor room temperature. Therefore, the vacuum PV glazing contributes to stabilising the temperature of the indoor environment despite the fluctuating solar radiation and periodic outdoor temperature. It is suggested that the vacuum PV glazing has the potential to enhance the climate adaptability of BIPV windows under different climate backgrounds.

Keywords: building integrated photovoltaic (BIPV); vacuum glazing; semi-transparent photovoltaic; heat transfer behaviours; energy flow

check for updates

Academic Editor: Cinzia Buratti

Received: 11 April 2025 Revised: 8 June 2025 Accepted: 14 June 2025 Published: 23 July 2025

Citation: Qiu, C.; Yang, H.; Dong, K. Dynamic Heat Transfer Modelling and Thermal Performance Evaluation for Cadmium Telluride-Based Vacuum Photovoltaic Glazing. *Buildings* 2025, 15, 2612. https://doi.org/10.3390/buildings15152612

Copyright: © 2025 by the authors. Licensee MDPI, Basel, Switzerland. This article is an open access article distributed under the terms and conditions of the Creative Commons Attribution (CC BY) license (https://creativecommons.org/licenses/by/4.0/).

1. Introduction

Although the Paris Agreement announced the pursuit of the "1.5 $^{\circ}$ C climate limit" goal by the end of this century, it was reported that the period from February 2023 to January 2024 was the first 12-month period in which global warming exceeded 1.5 $^{\circ}$ C [1,2].

With this level of warming, extreme weather events, such as heat waves, intense rainfalls, and extreme storms, have been observed with an increase in frequency and severity [3]. To limit global temperature rise within the threshold, it requires a tremendous effort from all sectors to mitigate greenhouse gas (GHG) emissions. The building sector is responsible for over 40% of energy consumption and one-third of GHG emissions globally [4]. Therefore, building transformation towards green and sustainability plays a critical role in climate change mitigation strategies. On the pathway to carbon neutrality in the building sector, photovoltaic (PV) integration offers a promising solution due to the benefit of renewable energy production on-site [5].

With the rapid development of solar cell material, the applications of photovoltaic technology in buildings have evolved from building-attached photovoltaics (BAPVs) to building-integrated photovoltaics (BIPVs) [6]. The most common BAPV application is rack-mounted or standoff arrays of PV modules on rooftops using the first-generation solar cells, such as mono-crystalline PV cells and poly-crystalline PV cells [7]. Compared with BAPV applied on the limited area of roofs, BIPV applications on building facades have a larger potential for renewable energy utilisation, especially for high-rise buildings [8]. Moreover, a well-designed BIPV system contributes to indoor thermal and visual comfort since it integrates into the building structure by substituting conventional materials in part of the building envelope [9]. Nowadays, due to the semi-transparent appearance, the second-generation solar cells, including amorphous silicon (a-Si), cadmium telluride (CdTe), and copper indium gallium selenide (CIGS) PV cells, are introduced into BIPV systems, such as semi-transparent photovoltaic (STPV) windows and photovoltaic double skin façade (PV-DSF) for the benefit of aesthetic appeal and visual comfort [10,11]. In terms of the thermal aspect, the most prominent characteristic of BIPV windows is the relatively high solar heat gain control ability [12]. However, the thermal insulation of typical STPV glazings, such as single PV windows and double PV windows, is inadequate for the heating-dominated regions [13,14]. On the other hand, due to the poor thermal insulation capability of the conventional PV glazings, the waste heat gain absorbed by the solar cells would substantially transfer indoors, thereby increasing the cooling energy consumption in the cooling season [15,16].

To enhance climate adaptability, a novel vacuum PV glazing system was proposed to combine the advantages of STPV window and vacuum glazing, thereby improving the thermal insulation capability of BIPV applications [17]. The first generation of this novel BIPV window was designed as an a-Si-based vacuum PV glazing with a four-layer structure. An outdoor test was conducted to investigate its electrical characterisation [18], and the simulation study on the annual energy performance found that the vacuum PV glazing could improve the thermal performance and save cooling energy in Hong Kong [17]. In terms of daylighting and energy performance, further study was conducted to investigate this application's adaptability and limitations under various climate conditions [19]. Based on the above research and development, a novel cadmium telluride (CdTe)-based vacuum PV glazing was proposed and developed [20], which is lighter and thinner as a three-layer structure. Huang et al. [21,22] conducted field experiments and numerical modelling on a photovoltaic vacuum glazing and a hollow photovoltaic vacuum glazing. The results suggested that both types of PV vacuum glazing are beneficial in saving cooling and heating energy compared to the double-glazed glass. Similar research on the energy-saving performance of a PV combined hybrid vacuum glazing (PVCHVG) was conducted by Uddin et al. [23]. It was found that the PVCHVG can save the overall energy consumption up to 59.39% and 76.33% in the heating-dominated regions and cooling-dominated regions. Ghosh et al. [24,25] fabricated a PV-vacuum glazing consisting of a multi-crystalline (mc-Si) PV solar cell, a single glass, and a vacuum glazing from NSG SPACIA. The outdoor

tests showed that the overall heat transfer coefficient (U-value) of the PV-vacuum glazing was 0.8 W/m²K, and the solar heat gain coefficient (SHGC) was 0.42. Jarimi et al. [26] manufactured two lab-scale prototypes of the vacuum-insulated a-Si PV glazing, namely, PV VG-2L. The average U-value was determined from a validated steady-state heat transfer model, reported as 0.60 W/m²K. Zhang et al. [27] investigated the thermal performance of the vacuum PV glazing (VPV-IGU) and the vacuum glazing integrated with PV double-skin façade (VPV-DSV). It was found that the VPV-IGU had a better thermal insulation performance. The U-value of VPV-IGU was 0.944 W/m²K, which is lower than the U-value of VPV-DSV at 1.138 W/m²K.

The previous research shows the significant potential of the application of the vacuum PV glazing in terms of thermal performance and energy saving under different climatic conditions. In terms of heat transfer modelling of the vacuum PV glazing, Chen et al. [28] conduct a numerical model based on COMSOL Multiphysics V5.2 under steady-state conditions to investigate the thermal insulation performance of a 4-layer a-Si-based PV vacuum glazing by determining the overall U-value for a given condition. However, the reliability of this model has not been verified through experiments with an actual sample. Tan et al. [29] developed and validated a one-dimensional (1D) steady-state heat transfer model for the vacuum-PV glazing (VPV) by using the simplified thermal node assumption. A static U-value of the VPV was calculated as 0.89 W/m²K. Similarly, Radwan et al. [30] estimated the U-value of different types of vacuum PV glazing using the ANSYS model (ANSYS FLUENT 12.0) under a steady-state boundary condition. Although the aforementioned 1D or 3D steady-state heat transfer model of the vacuum PV glazing can estimate the key thermal performance indicators under a specific condition, those thermal modelling methods cannot be used to investigate the dynamic heat transfer behaviour of this novel BIPV glazing under real-world conditions. To be specific, the dynamic heat transfer process of the vacuum PV glazing involves solar radiation absorption, reflection, and transmission, heat conduction through each component, radiation-dominant heat transfer between the vacuum gap, transient heat transfer with indoor and outdoor environments, and the effect of solar power transformation.

Regarding mathematical thermal modelling methods for different types of BIPV windows, simplified assumptions were commonly used to reduce the complexity, such as a constant radiative heat transfer coefficient between layers [31], simplification of the solar absorption process in the transparent material [32], and a simplified resistance capacity network [33]. Infield et al. [34] presented a simplified heat transfer model for an integrated ventilated PV façade based on an extension of the U-value and g-value. The hourly steadystate U-values and g-values could be calculated and substituted into the energy balance model to determine the monthly net energy gains and effective thermal coefficient. However, this method relies on static U-values and g-values, which are unsuitable for dynamic conditions. Chow et al. [32] first introduced a one-dimensional transient energy model for a semi-transparent a-Si PV ventilated window. However, this transient heat transfer model assumed the radiative heat transfer was proportional to the temperature difference, where a constant radiative heat transfer coefficient was applied. Therefore, there are deviations in the calculation that cannot be ignored when the temperature difference of the radiative heat transfer is relatively large. Moreover, the solar absorption in the glass was simply represented by a constant value of heat absorptance. Hence, the heat effect due to solar absorption can only be determined at the surfaces of each layer, while the dynamic process of heat generation due to solar radiation within the glass was ignored. Similar methods were also adopted to investigate the thermal performance of a double-skin ventilated window integrated with CdTe cells (CdTe-DSV) [35], and an integrated vacuum glazing with PV double-skin ventilated window (VPV-DSV) [27,36]. Ding and Yu [33] developed a

Buildings **2025**, 15, 2612 4 of 33

1D transient heat balance mathematical model for the STPV-IGU based on the simplified resistance-capacity (RC) network method. However, this model can only calculate results for the specific temperature nodes, thus simplifying the temperature distribution of the PV glazing.

Due to the complexity of the dynamic thermal behaviours of the vacuum PV glazing, a comprehensive transient model should be developed and applied to accurately simulate the solar absorption in each layer, quantify radiative heat transfer, particularly in the vacuum cavity, and capture time-dependent thermal dynamics that account for time-varying boundary conditions. To address these challenges, this study conducts a comprehensive investigation on the complex heat transfer behaviours of the three-layer CdTe-based vacuum PV glazing by adopting dynamic modelling. Section 2 presents the methodology of the dynamic heat transfer modelling for the CdTe-based vacuum PV glazing. Firstly, the structure of the vacuum PV glazing was introduced in detail. Then, a comprehensive transit heat transfer model was developed, and the corresponding numerical solutions were established using the explicit finite difference method. As a result, the temperature profile and the transit heat transfer of the vacuum PV glazing can be obtained dynamically under real-world operational scenarios. In Section 3, the experimental work was conducted to validate the reliability and accuracy of the developed heat transfer model. Section 4 analyses the dynamic heat transfer behaviour and thermal performance of the vacuum PV glazing. The transit heat transfer model is applied to investigate the temperature variations, energy flows, dynamic thermal characteristics, and net heat flux under different scenarios. Section 5 summarizes the main findings of this study, potential applications in real practice, and future work. This study contributes to revealing the heat transfer mechanism and dynamic thermal performance of this novel CdTe-based vacuum PV glazing.

2. Materials and Methodology

2.1. Structure of the CdTe-Based Vacuum PV Glazing

As shown in Figure 1, the proposed vacuum PV glazing integrates a vacuum glazing as the backplate into a CdTe PV glazing with a superstrate configuration. A stack of thin-film photovoltaic layers is encapsulated between a glass with a transparent conducting oxide (TCO) coating and a vacuum glazing. The vacuum glazing comprises two glass sheets and a 0.1 mm evacuated gap. Within the vacuum gap, the small support pillars are uniformly positioned to provide structural support against the atmospheric pressure. Consequently, the CdTe-based vacuum PV glazing consists of a TCO glass and two glasses forming a three-layer structure. The CdTe-based PV module converts solar energy into electrical output. Meanwhile, the vacuum gap serves as an effective heat insulator, which eliminates the heat conduction and convection through the glazing. The front view and side view of the CdTe-based vacuum PV glazing are shown in Figure 2. The dimension of the sample is 300 mm \times 300 mm \times 15 mm (L \times W \times H). This specific sample was manufactured by ASP, a thin-film PV manufacturer in Hangzhou, China. The front view of the sample shows that the vacuum PV glazing can provide a certain amount of daylight availability. The side view clearly demonstrates the three-layer structure of the vacuum PV glazing.

Buildings **2025**, 15, 2612 5 of 33

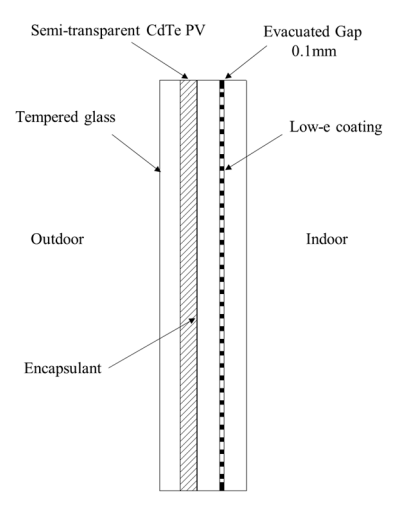


Figure 1. Structure of the CdTe-based vacuum PV glazing.

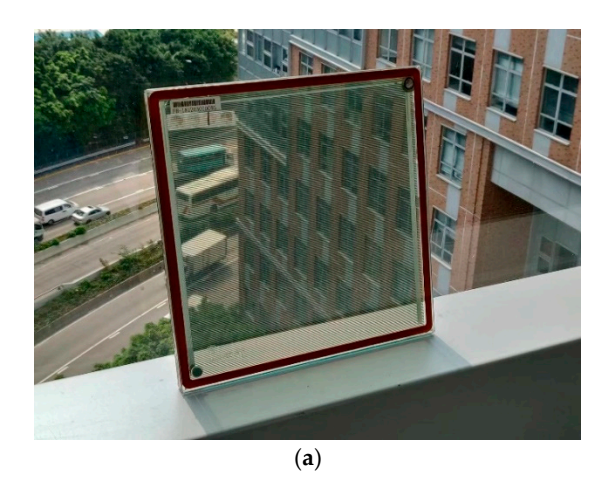




Figure 2. The pictures of the CdTe-based vacuum PV glazing with three-layer structure. (a) Front view; (b) Side view.

2.2. Transient Heat Transfer Model

2.2.1. Heat Transfer Mechanism

To examine the dynamic heat transfer process of the vacuum PV glazing in detail, a comprehensive one-dimensional heat transfer model has been established in this research. The model incorporates various factors, including transient conductive heat transfer through the transparent substance, specific heat transfer behaviour of the vacuum glazing and the PV glazing, as well as radiative and convective heat transfer occurring between the exterior/interior surface and the outdoor/indoor environment. Furthermore, this study also considered the dynamic PV power generation when solar energy is available.

The dimensions of the mathematical model for the vacuum PV glazing are illustrated in Figure 3. The x-axis indicates the direction from indoor to outdoor, aligned with the glazing thickness. The internal surface is denoted by x = 0, while the external surface corresponds to x = L. Figure 4 illustrates the general heat transfer mechanism of the vacuum PV glazing. When the incident solar radiation passes through the transparent substance, the solar energy is attenuated as long as the long-wave radiation is absorbed by the material. Of particular note is that the absorbed solar heat by the solar cells causes their temperature to be higher than that of the adjacent glass panes. Therefore, there is conductive heat transfer from the PV cells to both sides during the daytime. For the CdTe PV glazing, the PV layer is formed as a large amount of laser-cutting small pieces of solar cells apart at a small distance. In this case, it is assumed that the absorbed heat uniformly

Buildings **2025**, 15, 2612 6 of 33

transfers to adjacent substances. Due to the heat insulation ability of the vacuum gap, the radiative heat transfer dominates the thermal exchange between the glass sheets of the vacuum glazing. The previous study indicates that the effect of the support pillars on the total heat flux is at most 1% since the conductance accounts for only $0.01~\text{W/(m}^2\text{K)}$ [37]. Consequently, it is assumed that the conductive and convective heat through the vacuum gap is minimised to a negligible level. Based on the above discussion, several proper assumptions are made as follows:

- (1) The solid substances within the glazing are isotropic and possess constant optical and thermal properties.
- (2) The perimeter of the glazing is adiabatic.
- (3) The temperature of each glass surface is uniform.
- (4) The widths of the PV solar cells and the vacuum gap are considered negligibly small.
- (5) The absorbed heat of the PV solar cells is assumed to transfer to the adjacent substances with uniform temperatures.
- (6) The thermal conduction and convection through the vacuum gap are negligible.

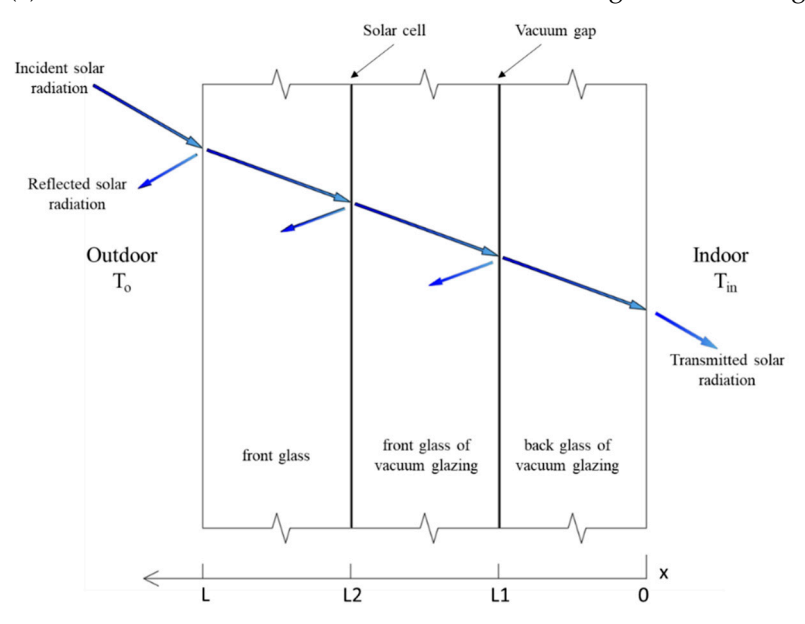


Figure 3. Schematic of the mathematical model for vacuum PV glazing.

(a) For the front glass (where $L_2 < x < L$)

As mentioned before, the first layer of the vacuum PV glazing is a TCO glass, which serves as the superstrate of the CdTe PV solar cells. When solar irradiation penetrates the glass, it divides into three parts: the first part is reflected at the external surface, the second part is absorbed by the material and converted into internal heat energy, and the remaining part passes through the glass as the transmitted solar energy. The energy balance equation takes into account the transient heat conduction and solar energy attenuation in the glass, as shown in Equation (1).

$$\rho C_p \frac{\partial T_{fg}(x,t)}{\partial t} = \lambda_{fg} \frac{\partial^2 T_{fg}(x,t)}{\partial x^2} + \frac{dF_{fg}}{dx}$$
 (1)

where the subscript fg represents the layer of the front glass; T(x,t) is the node temperature of the front glass at distance x and time t; ρ is the density of the substance; C_p and λ are the specific heat capacity (J/(kgK)) and the thermal conductivity (W/(mK)), respectively;

Buildings **2025**, 15, 2612 7 of 33

F is the attenuated function of the solar energy in the transparent material, which can be estimated by the following equation:

$$F_{fg}(x) = G \exp\left[\frac{-S_{fg}(L-x)}{\cos \theta_2}\right]$$
 (2)

where G is the total incident solar irradiation on the window (W/m²), and S is the extinction coefficient (m⁻¹). The total incident solar irradiation consists of two components, the direct and diffuse solar irradiation, which is given as follows:

$$G = I_{dir}\cos\theta_1 + I_{dif} \tag{3}$$

where I_{dir} and I_{dif} are direct solar irradiation (W/m²) and the diffuse solar irradiation (W/m²), respectively; θ_1 and θ_2 represent the incidence angle and refraction angle of the beam solar irradiation, respectively. According to Snell's law, the relationship between the incidence angle and refraction angle is given by the following:

$$\theta_2 = \sin^{-1} \left[\frac{n_1}{n_2} \sin \theta_1 \right] \tag{4}$$

where n_1 is the refractive index of air; n_2 is the refractive index of glass.

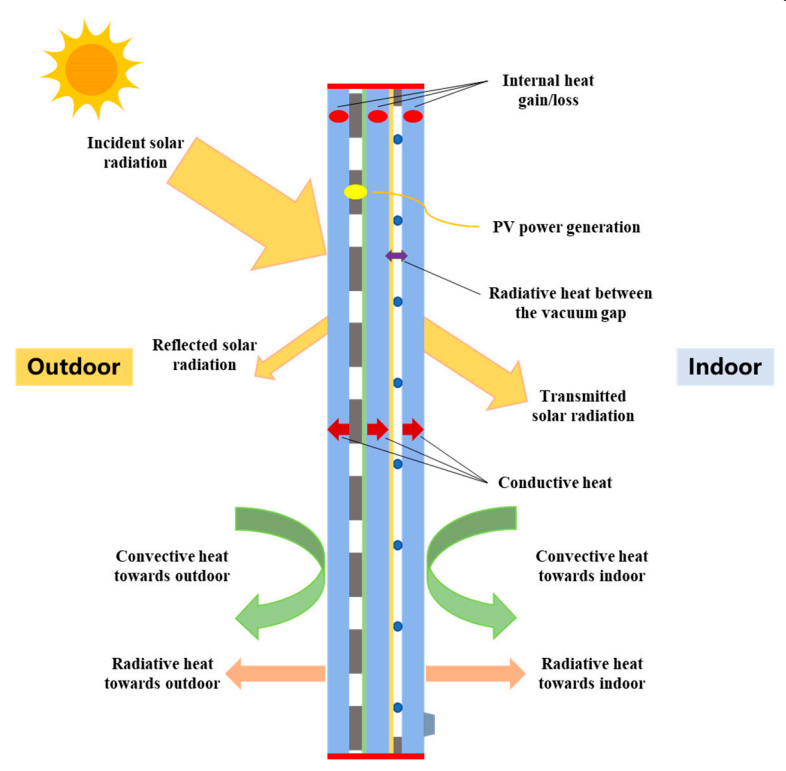


Figure 4. The heat transfer mechanism of the vacuum PV glazing.

(b) Solar cell $(x = L_2)$

The solar cells absorb the incoming solar energy and convert a portion of it into electricity. Meanwhile, the PV temperature increases as a result of the internal heat gain from the remaining absorbed solar energy. A certain amount of solar energy passes through the PV layer due to the semi-transparency of the CdTe solar cells and the distance between them. Equation (5) represents the energy balance equation for the solar cells ($x = L_2$).

$$\frac{A_{pv}}{A_g}\alpha_{pv}\tau_{fg}G - \eta_{pv}G = \lambda_{fvg}\frac{\partial T_{fvg}(x,t)}{\partial x} - \lambda_{fg}\frac{\partial T_{fg}(x,t)}{\partial x}$$
 (5)

where A_{pv} and A_g are the area of the PV solar cells and the total area of the glazing (m²), respectively; α_{pv} and η_{pv} are the absorbance and the conversion efficiency of the PV cells, respectively; τ_{fg} is the transmittance of the front glass.

The dynamic conversion efficiency of CdTe PV cells is determined by the conversion efficiency at the standard test condition η_{STC} and the operating temperature T_{pv} , which is given by Equation (6):

$$\eta_{pv} = \eta_{STC} [1 - \beta_{pv} (T_{pv} - T_{STC})] \tag{6}$$

where β_{pv} is the temperature coefficient of the solar cells; T_{STC} is the standard test operating temperature. Consequently, the model dynamically integrates the heat transfer process and the renewable energy generation of the vacuum PV glazing.

(c) Front glass of the vacuum glazing $(L_1 < x < L_2)$

The energy balance equation in the front glass of the vacuum glazing ($L_1 < x < L_2$) can be described as follows:

$$\rho C_p \frac{\partial T_{fvg}(x,t)}{\partial t} = \lambda_{fvg} \frac{\partial^2 T_{fvg}(x,t)}{\partial x^2} + \frac{dF_{fvg}}{dx}$$
 (7)

where the subscript fvg represents the layer of the front glass of the vacuum glazing. Similarly, the solar energy attenuated function F_{fvg} is given by the following:

$$F_{fvg}(x) = \tau_{fg}G' \exp\left[\frac{-S_{fvg}(L_2 - x)}{\cos \theta_2}\right]$$
 (8)

where $\tau_{fg}G'$ is the incident solar radiation on the front glass of the vacuum glazing. The term G' can be calculated as follows:

$$G' = \frac{\tau_{pv}GA_{pv} + GA_r}{A_g} \tag{9}$$

This term (G') represents the average transmitted solar radiation through the solar cells and the rest area, A_r (m^2).

(d) Vacuum gap $(x = L_1)$

The presence of the vacuum gap results in thermal radiation dominating the heat transfer between the front and back glass of the vacuum glazing. Therefore, the energy balance equation at the inner surface of the front glass and the outer surface of the back glass of the vacuum glazing can be expressed as follows:

$$-\lambda_{fvg} \frac{\partial T_{fvg}(x,t)}{\partial x} = \varepsilon_s \sigma [(T_{fvg}(L_1,t))^4 - (T_{bvg}(L_1,t))^4]$$
(10)

$$-\lambda_{bvg} \frac{\partial T_{bvg}(x,t)}{\partial x} = \varepsilon_s \sigma [(T_{bvg}(L_1,t))^4 - (T_{fvg}(L_1,t))^4]$$
(11)

where σ is the Stefan–Boltzmann constant, which is 5.67 \times 10⁻⁸ W/(m²K⁴); ε_s is the effective emissivity of the glass sheets, which is calculated by the following:

$$\varepsilon_s = \frac{1}{\frac{1}{\varepsilon_1} + \frac{1}{\varepsilon_2} - 1} \tag{12}$$

where ε_1 and ε_2 are the emissivities of the inner surface and the outer surface beside the vacuum gap, respectively.

(e) Back glass of the vacuum glazing $(0 < x < L_1)$

The following equation describes the energy balance in the back glass of the vacuum glazing (0 < x < L_1):

$$\rho C_p \frac{\partial T_{bvg}(x,t)}{\partial t} = \lambda_{bvg} \frac{\partial^2 T_{bvg}(x,t)}{\partial x^2} + \frac{dF_{bvg}}{dx}$$
(13)

where the subscript bvg represents the layer of the back glass of the vacuum glazing. The solar energy attenuated function F_{bvg} is defined as follows:

$$F_{bvg}(x) = \tau_{fg}\tau_{fvg}G'\exp\left[\frac{-S_{bvg}(L_1 - x)}{\cos\theta_2}\right]$$
 (14)

2.2.2. Boundary Conditions

In this heat transfer model, the boundary conditions integrate the convection and the radiation heat exchange between the outside/inside surfaces of the vacuum PV glazing and the outdoor/indoor environment. For the outside surface (x = L) and the inside surface (x = 0), the energy balance can be expressed by the following equations:

$$-\lambda_{fg} \frac{\partial T_{fg}(L,t)}{\partial x} = h_o [T_{fg}(L,t) - T_o] + \varepsilon_{fg} \sigma [(T_{fg}(L,t))^4 - T_o^4]$$
(15)

$$-\lambda_{bvg} \frac{\partial T_{bvg}(0,t)}{\partial x} = h_i [T_{bvg}(0,t) - T_{in}] + \varepsilon_{bvg} \sigma [(T_{bvg}(0,t))^4 - T_{in}^4]$$
(16)

where $T_{fg}(L,t)$ and $T_{bvg}(0,t)$ are the outside and inside surface temperature of the vacuum PV glazing, respectively; T_0 and T_{in} are the outdoor and indoor temperature, respectively; ε represents the emissivity of the corresponding material; h_0 and h_i are the convective heat transfer coefficient on the outside and inside surface of the vacuum PV glazing, respectively, which are given by [38,39] the following:

$$h_0 = 5.34 + 3.27v \tag{17}$$

$$h_i = 1.46 \left(\frac{\left| T_{bvg}(0, t) - T_{in} \right|}{H} \right)^{0.25} \tag{18}$$

where v is the wind speed (m/s) and H is the height of the vacuum PV glazing.

It is worth noting that the convective heat flux Q_c and the radiative heat flux Q_r through the window can be derived from Equation (16), which are determined as follows:

$$Q_c = h_i [T_{hvo}(0, t) - T_{in}] \tag{19}$$

$$Q_r = \varepsilon_{bvg} \sigma [(T_{bvg}(0,t))^4 - T_{in}^4]$$
(20)

The total heat gain of the vacuum PV glazing can be expressed by the following:

$$Q_{total} = Q_c + Q_r + Q_s \tag{21}$$

where Q_s is the transmitted solar radiation through the vacuum PV glazing. The PV coverage should be taken into consideration when calculating the direct transmitted solar radiation. Therefore, it is given by the following:

$$Q_s = \tau_{fg} \tau_{fvg} \tau_{bvg} G' \tag{22}$$

2.2.3. Initial Conditions

For the start time (t = 0) of the dynamic mathematical model, it is assumed that the temperature profile along the thickness of the vacuum PV glazing follows a linear distribution, which depends on the indoor and outdoor air temperature. Therefore, the initial conditions for the start of iteration are defined by the following equation:

$$T(x,0) = \frac{T_0 - T_{in}}{I} \cdot x + T_{in}$$
 (23)

where T(x,0) represents the temperature of all nodes when t=0.

2.2.4. Numerical Solutions

Since the boundary conditions combine the convective and radiative heat transfer, the equations are non-linear and difficult to solve with analytical solutions. The explicit finite difference method (FDM) is used to solve the partial differential equations by approximating the partial derivatives with finite differences. Expressing Equations (1)–(19) in discrete form with $x = i\Delta x$, $t = k\Delta t$, the term $(T)_i^k$ denotes the temperature at the ith node when the number of the time step is k. Therefore, for the front glass ($L_2 < x < L$), the temperature $(T_{fg})_i^{k+1}$ is calculated by the following:

$$(T_{fg})_{i}^{k+1} = (1 - 2Fo)(T_{fg})_{i}^{k} + Fo[(T_{fg})_{i-1}^{k} + (T_{fg})_{i+1}^{k}] + \frac{S_{fg}G\Delta t}{\rho C_{p}} \exp[\frac{-S_{fg}(L - i\Delta x)}{\cos \theta_{2}}]$$
(24)

where i is the node number; k is the time step; Δx is the distance interval; Δt is the time interval for iteration; Fo is the Fourier number, which can be calculated by the following:

$$Fo = \frac{\lambda \Delta t}{\rho C_p \Delta x^2} \tag{25}$$

The Fourier number is a dimensionless number that represents the ratio of the heat conduction rate to the rate of thermal energy storage. To ensure the convergence of iteration, the stability condition implied in the equation is that *Fo* should be less than 0.5.

Similarly, the explicit finite difference method was applied to solve the equations for different layers of the vacuum PV glazing. For Equation (5) at $x = L_2$, the temperature of the solar cells $(T_{pv})_{i(L_2)}^{k+1}$ is solved as follows:

$$(T_{pv})_{i(L_2)}^{k+1} = \frac{\Delta x}{\lambda_{fg} + \lambda_{fvg}} (\frac{A_{PV}}{A_g} \tau_{fg} \alpha_{pv} - \eta_{pv}) G + \frac{1}{\lambda_{fg} + \lambda_{fvg}} [\lambda_{fvg} (T_{fvg})_{i(L_2)-1}^{k+1} + \lambda_{fg} (T_{fg})_{i(L_2)+1}^{k+1}]$$
(26)

where $i(L_2) = L_2/\Delta x$, which denotes the node number of the distance L_2 .

For the front glass of the vacuum glazing ($L_1 < x < L_2$), the solution should be as follows:

$$(T_{fvg})_{i}^{k+1} = (1 - 2Fo)(T_{fvg})_{i}^{k} + Fo[(T_{fvg})_{i-1}^{k} + (T_{fvg})_{i+1}^{k}] + \frac{S_{fvg}\tau_{fg}G'\Delta t}{\rho C_{v}} \exp[\frac{-S_{fvg}(L_{2} - i\Delta x)}{\cos\theta_{2}}]$$
(27)

By solving the equations for the heat transfer between the vacuum gap, the temperature of the front glass of vacuum glazing, at surface $x = L_1$, can be obtained by the following:

$$(T_{fvg})_{i(L_{1})}^{k+1} = (1 - 2Fo)(T_{fvg})_{i(L_{1})}^{k} + 2Fo(T_{fvg})_{i(L_{1})+1}^{k} + \frac{2\Delta t}{\rho C_{p}\Delta x} \{\varepsilon_{s}\sigma[((T_{fvg})_{i(L_{1})}^{k})^{4} - ((T_{fvg})_{i(L_{1})}^{k})^{4}]\} + \frac{S_{fvg}\tau_{fg}G'\Delta t}{\rho C_{p}} \exp[\frac{-S_{fvg}(L_{2}-i\Delta x)}{\cos\theta_{2}}]$$
(28)

At surface $x = L_1$, the temperature of the back glass of vacuum glazing can be obtained by the following:

$$(T_{bvg})_{i(L_1)}^{k+1} = (1 - 2Fo)(T_{bvg})_{i(L_1)}^{k} + 2Fo(T_{bvg})_{i(L_1)-1}^{k} + \frac{2\Delta t}{\rho C_p \Delta x} \{ \varepsilon_s \sigma [((T_{fvg})_{i(L_1)}^k)^4 - ((T_{fvg})_{i(L_1)}^k)^4] \} + \frac{S_{bvg} \tau_{fg} \tau_{fvg} G' \Delta t}{\rho C_p} \exp [\frac{-S_{bvg}(L_1 - i\Delta x)}{\cos \theta_2}]$$
(29)

For the back glass of the vacuum glazing $(0 < x < L_1)$, the solution should be as follows:

$$(T_{bvg})_{i}^{k+1} = (1 - 2Fo)(T_{bvg})_{i}^{k} + Fo[(T_{bvg})_{i-1}^{k} + (T_{bvg})_{i+1}^{k}] + \frac{S_{fvg}\tau_{fg}\tau_{fg}\sigma_{fvg}G'\Delta t}{\rho C_{p}} \exp[\frac{-S_{bvg}(L_{1} - i\Delta x)}{\cos\theta_{2}}]$$
(30)

The boundary conditions, Equations (15) and (16), are also solved by the explicit finite difference method. The temperatures at the exterior surface and interior surface of the vacuum PV glazing can be expressed as follows.

For the exterior surface (x = L), the solution is calculated by:

$$(T_{fg})_{i(L)}^{k+1} = (1 - 2Fo - 2Fo \cdot Bi, o)(T_{fg})_{i(L)}^{k} + 2Fo(T_{fg})_{i(L)-1}^{k} + 2Fo \cdot Bi, oT_{o}^{k} + \frac{2\Delta t}{\rho C_{p}\Delta x} \{\varepsilon_{fg}\sigma[(T_{o}^{k})^{4} - ((T_{fg})_{i(L)}^{k})^{4}]\} + \frac{S_{fg}G\Delta t}{\rho C_{p}} \exp[\frac{-S_{fg}(L - i\Delta x)}{\cos \theta_{2}}]$$
(31)

For the interior surface (x = 0), the solution is determined by:

$$(T_{bvg})_{0}^{k+1} = (1 - 2Fo - 2Fo \cdot Bi, in)(T_{bvg})_{0}^{k} + 2Fo(T_{bvg})_{1}^{k} + 2Fo \cdot Bi, inT_{i}^{k} + \frac{2\Delta t}{\rho C_{v} \Delta x} \{ \varepsilon_{bvg} \sigma [(T_{i}^{k})^{4} - ((T_{fvg})_{0}^{k})^{4}] \} + \frac{S_{bvg} \tau_{fg} \tau_{fvg} G' \Delta t}{\rho C_{v}} \exp[\frac{-S_{bvg}(L_{1} - i\Delta x)}{\cos \theta_{2}}]$$
(32)

where *Bi*, *o* and *Bi*, *in* are the Biot numbers regarding the convective heat transfer coefficient of the exterior surface and interior surface, respectively. The expression of the Biot number is given by the following:

$$Bi = \frac{h\Delta x}{\lambda} \tag{33}$$

In this study, Matlab was used to develop the dynamic heat transfer model for the vacuum PV glazing. By applying Equations (24)–(33), the temperature profile across the vacuum PV glazing can be determined for given boundary conditions. Subsequently, after obtaining the inside surface temperature at each time step, the heat gain or heat loss through the vacuum PV glazing can be calculated using Equations (19)–(22).

3. Experiment and Model Validation

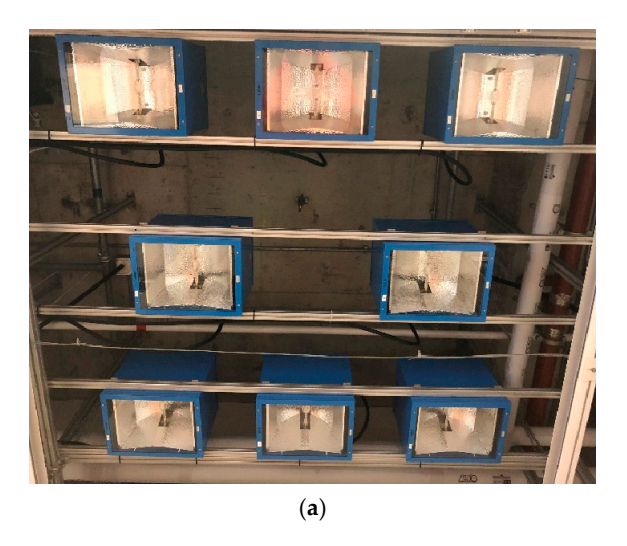
To ensure the reliability and accuracy of the developed transient heat transfer model for the CdTe-based vacuum PV glazing, a comprehensive validation process was conducted by comparing simulation results with experimental data. In this section, the experimental setup, statistical validation metrics, and analysis of results are presented in detail to demonstrate the model's capability to reveal the dynamic thermal behaviour of the vacuum PV glazing under unsteady conditions.

3.1. Experimental Setup and Conditions

A validation experiment was designed to validate the developed heat transfer model and evaluate the dynamic thermal performance of the vacuum PV glazing under controlled solar conditions. For the dynamic heat transfer model, the incident solar radiation, ambient temperature, and indoor temperature are the required boundary conditions. Therefore, those variables were measured as the inputs of the developed model during the test. On

the other hand, the outside and inside temperatures and heat flux through the glazing area were measured for the validation of simulation results.

The validation test was carried out at the Solar Simulation Laboratory of the Hong Kong Polytechnic University. As illustrated in Figure 5a, a solar irradiation system incorporated eight Hönle SOL-2000 high-intensity lamps (manufacturer: Dr. Hönle AG, Gilching, Germany)for the test, which complies with the International Standard IEC 60904-9 [40]. This system ensured stable and uniform artificial irradiation while minimizing spectral deviation from natural sunlight. Two identical test rigs with the dimensions of 300 mm \times 300 mm \times 450 mm (L \times W \times H) were constructed, as shown in Figure 5b. A 300 mm \times 300 mm CdTe-based vacuum PV glazing sample was mounted horizontally on one test rig. The second test rig served as a reference point for the measurement of the incident solar radiation.



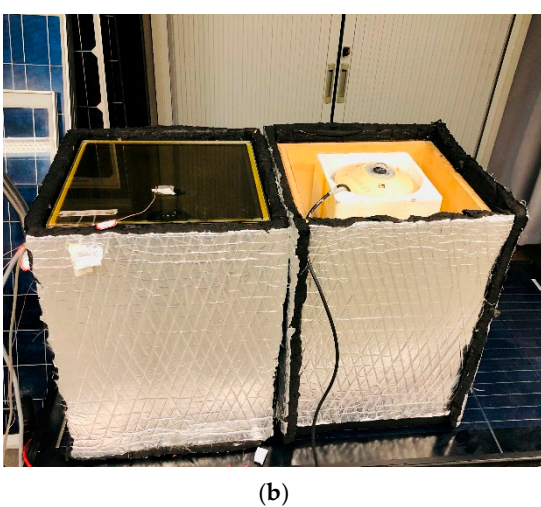


Figure 5. Validation experiment setup. (a) Solar simulation system; (b) Test rigs.

The validation test employed a high-precision EKO MS-802 pyranometer (sensitivity: about 7 μ V/(W/m²); non-linearity < 0.2% at 1000 W/m²) behind the glazing panel in the first test rig to measure transmitted solar radiation, and another pyranometer placed at the same height of the glazing outer surface to record incident solar radiation. Four T-type thermocouples (temperature range: from -50 °C to 400 °C; accuracy: ± 0.2 °C) were attached to the glazing's outer and inner surface, and to the air cavity inside and outside of the test rig to monitor temperature variations. A Captec RS-30 heat flux sensor (sensitivity: about 5 μ V/(W/m²); response time: 0.3 s) was placed at the center of the interior surface to measure heat gain through the vacuum PV glazing. All data were recorded at 10 s intervals using a multi-channel Graphtec GL840 data logger (range: 20 mV to 100 V; minimum resolution: 1 μ V and 0.1 °C), ensuring high-fidelity capture of the dynamic thermal behaviour of the vacuum PV glazing. The details of the optical, thermal, and electrical properties of each component of the CdTe-based vacuum PV glazing are shown in Table 1.

Table 1	Physical	characteristics	of the	CdTe-based	vacuum PV	olazino
Table 1.	. I HVSICAL	CHaracteristics	or the	Cu ie-baseu	. vacuum r v	giazilig.

Parameters	Value
Thermal conductivity of the glass panes (W/(mK))	1.38
Specific heat capacity of the glass panes (J/(kgK))	703
Density of the glass panes (kg/m^3)	2203
Extinction coefficient of the glass panes	23
Emissivity of the glass panes	0.85
Transmittance of the glass panes	0.77
Emissivity of the low-E coating	0.25
Transmittance of the CdTe PV solar cell	0.10
Absorptivity of the CdTe PV solar cell	0.79
PV coverage ratio	0.65
Efficiency of the CdTe PV solar cell	6.5%
Temperature coefficient of the CdTe PV solar cell (%/°C)	-0.214

As shown in Figure 6, during the validation test, the transmitted solar radiation of the vacuum PV glazing was recorded as $100 \pm 5 \, \text{W/m}^2$ against an incident solar radiation of approximately $800 \, \text{W/m}^2$. Therefore, the CdTe-based vacuum PV glazing shows an average direct solar transmission of 12.5%.

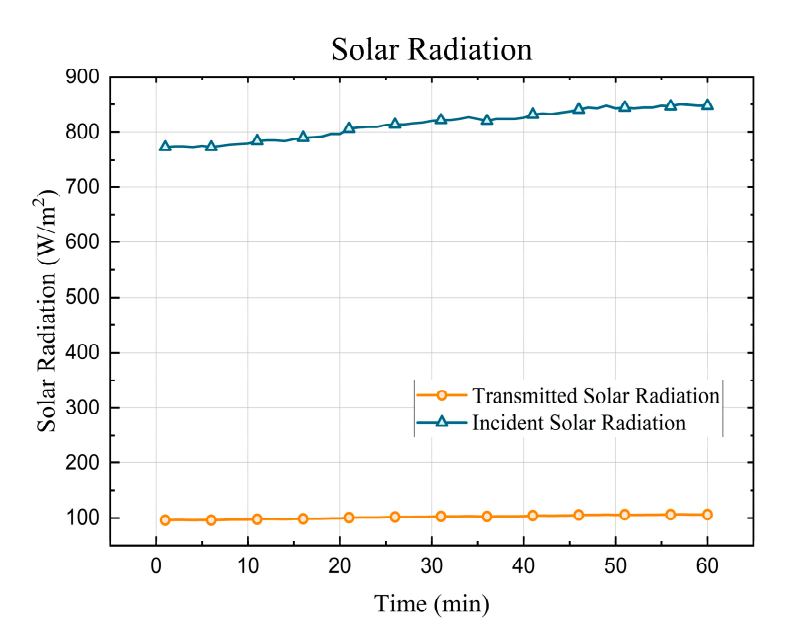


Figure 6. Measured incident and direct transmitted solar radiation.

3.2. Validation Results

To quantitatively assess the model's accuracy, three statistical metrics were adopted for the validation process, namely, root mean square error (RMSE), coefficient of variation of root mean square error (CvRMSE), and mean bias error (MBE). RMSE evaluated the absolute deviation between simulation results (P_i) and experimental data (R_i), where low RMSE values indicate high precision. CvRMSE normalises RMSE by the mean experimental dataset ($\overline{R_i}$), providing a relative measure of error. MBE identified overestimation when MBE > 0 or underestimation when MBE < 0. A near-zero MBE indicated negligible bias. The determination of these metrics is given by Equations (34)–(36) as follows:

$$RMSE = \sqrt{\frac{1}{N} \sum_{i=1}^{N} (P_i - R_i)^2}$$
 (34)

Buildings 2025, 15, 2612 14 of 33

$$CvRMSE(\%) = \frac{\sqrt{\frac{1}{N} \sum_{i=1}^{N} (P_i - R_i)^2}}{\frac{1}{N} \sum_{i=1}^{N} R_i}$$

$$MBE(\%) = \frac{\sum_{i=1}^{N} (P_i - R_i)}{\sum_{i=1}^{N} R_i}$$
(35)

$$MBE(\%) = \frac{\sum_{i=1}^{N} (P_i - R_i)}{\sum_{i=1}^{N} R_i}$$
 (36)

Figure 7a shows the inside and outside air temperature of the test rig, and the surface temperature profile of the vacuum PV glazing from both measurement and simulation. The ambient air temperature remained relatively stable at 26.5 \pm 0.5 $^{\circ}$ C, while the test rig's internal air temperature increased progressively from 29.0 °C to 33.4 °C. Although the measured outer surface of the vacuum PV glazing rose sharply from 31.6 °C to 66.8 °C after 1 h exposure to 800 W/m² solar radiation, the measured inner surface temperature varied from 27.7 °C to 41.7 °C. Since the inner surface temperature increased, the measured heat flux also increased from 18.9 W/m^2 to 75.6 W/m^2 , as shown in Figure 7b. The experimental results indicate that the interior surface temperature and indoor air temperature are quite stable compared with the exterior surface temperature of the vacuum PV glazing due to the excellent thermal insulation performance of the vacuum PV glazing.

As shown in Figure 7, the simulation results and measurement data align closely. The statistical validation also reveals minimal bias. The exterior surface temperature yielded a CvRMSE of 2.23% and MBE of -0.74%, while interior surface values showed a CvRMSE of 2.26% and MBE of -1.26%. For heat flux through the glazing area, simulations closely match experimental data, with a CvRMSE of 4.86% and MBE of -2.21%. These metrics confirm the model's high fidelity in predicting the thermal behaviour of the developed vacuum PV glazing under dynamic boundary conditions. Therefore, the validated model is able to resolve time-dependent thermal interactions, ensuring its reliability for analysing dynamic heat transfer processes and temperature distributions in the vacuum PV glazing under real-world operational scenarios. Table 2 shows the summary of the validation results.

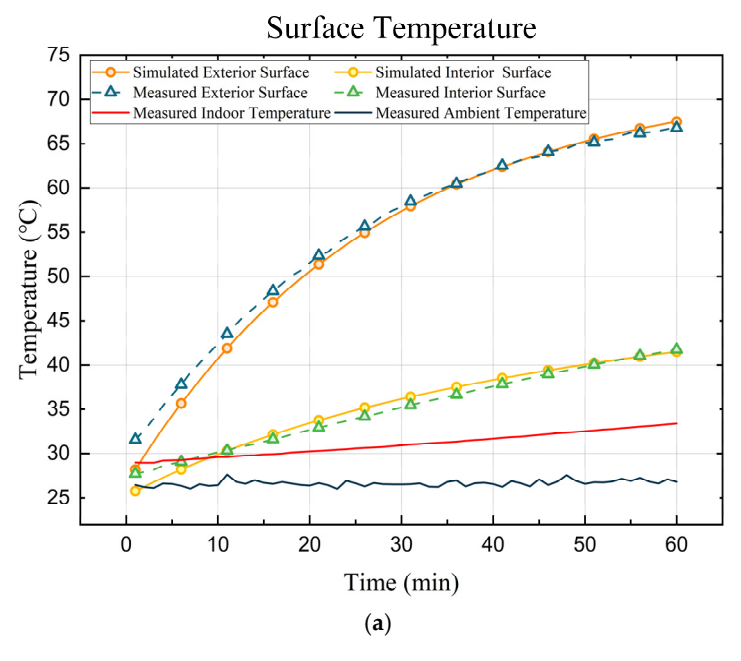


Figure 7. Cont.

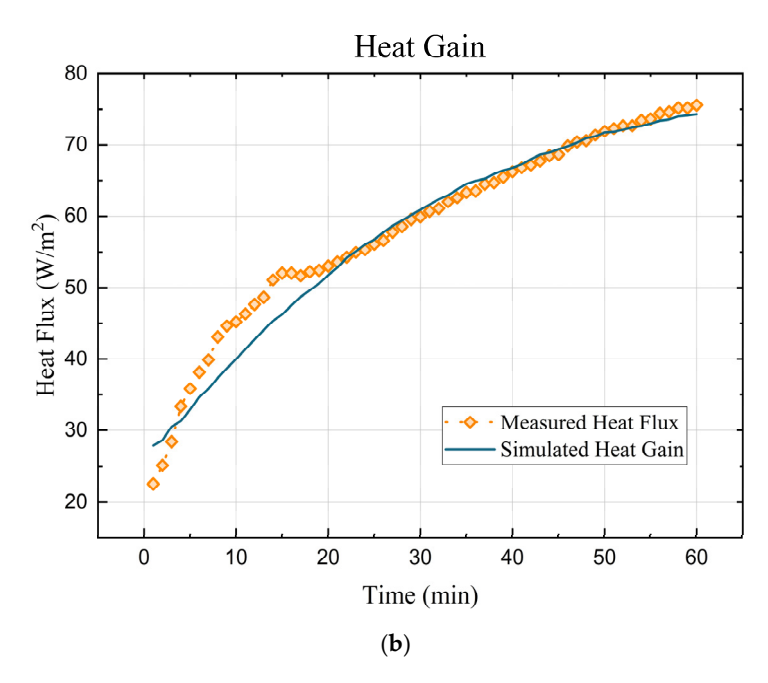


Figure 7. Comparison of the simulation results and experimental data. (a) Simulated and measured surface temperatures of the vacuum PV glazing; (b) Simulated and measured heat flux through the vacuum PV glazing.

Table 2. Validation metrics of model simulation results and experiment data.

Parameters	RMSE	CvRMSE	MBE
Exterior surface temperature	0.78 °C	2.23%	0.74%
Interior surface temperature	1.23 °C	2.26%	-1.26%
Heat gain	$2.6 \mathrm{W/m^2}$	4.55%	-1.30%

4. Results and Discussion

4.1. Dynamic Thermal Behaviour

For the vacuum PV glazing, thermal transmission is driven by the temperature gradient across the glazing surfaces and the absorption of solar energy by the glass panes and solar cells. Owing to the distinctive characteristics of the vacuum PV glazing, the solar cells absorb most of the incident solar radiation, and the vacuum gap efficiently suppresses the conductive and convective heat transfer. This study analyses the dynamic thermal behaviours of vacuum PV glazing under four different scenarios: summer daytime, summer nighttime, winter daytime, and winter nighttime. Table 3 outlines the specific boundary conditions for the simulations. The simulation runs 1 h for each scenario, with an iteration timestep of 0.5 s.

Table 3. Detailed conditions of four different scenarios.

Weather Conditions	Incident Solar Radiation (W/m²)	Outdoor Temperature (°C)	Indoor Temperature (°C)
Summer daytime	600	35	25
Summer nighttime	0	35	25
Winter daytime	300	-20	20
Winter nighttime	0	-20	20

4.1.1. Summer Conditions

During the summer daytime, the outdoor temperature exceeds the indoor temperature. The penetrating solar radiation significantly influences the overall heat transfer. Figure 8 illustrates the contouring isotherms and the 3-D isotherms of the vacuum PV glazing under the summer daytime conditions. The exterior surface, solar cells, vacuum gap, and interior surface are located at x = 1 mm, x = 5 mm, x = 10 mm, and x = 15 mm, respectively. Due to the higher absorptivity of the solar cells, a substantial portion of solar energy is absorbed, resulting in their higher temperature than the front glass. The heat absorbed by the solar cells is gradually released to the adjacent glass panes. It is found that the temperature of the solar cells and the exterior surface increases quickly, surpassing the outdoor temperature within 3 min. After this period, the net heat flux on the exterior surface is towards the outdoors. In this situation, the solar cell layer acts as a heat barrier, preventing heat transmittance driven by the indoor–outdoor temperature difference. Therefore, under the summer daytime conditions, the heat gain of the vacuum PV glazing mainly comes from the solar radiation.

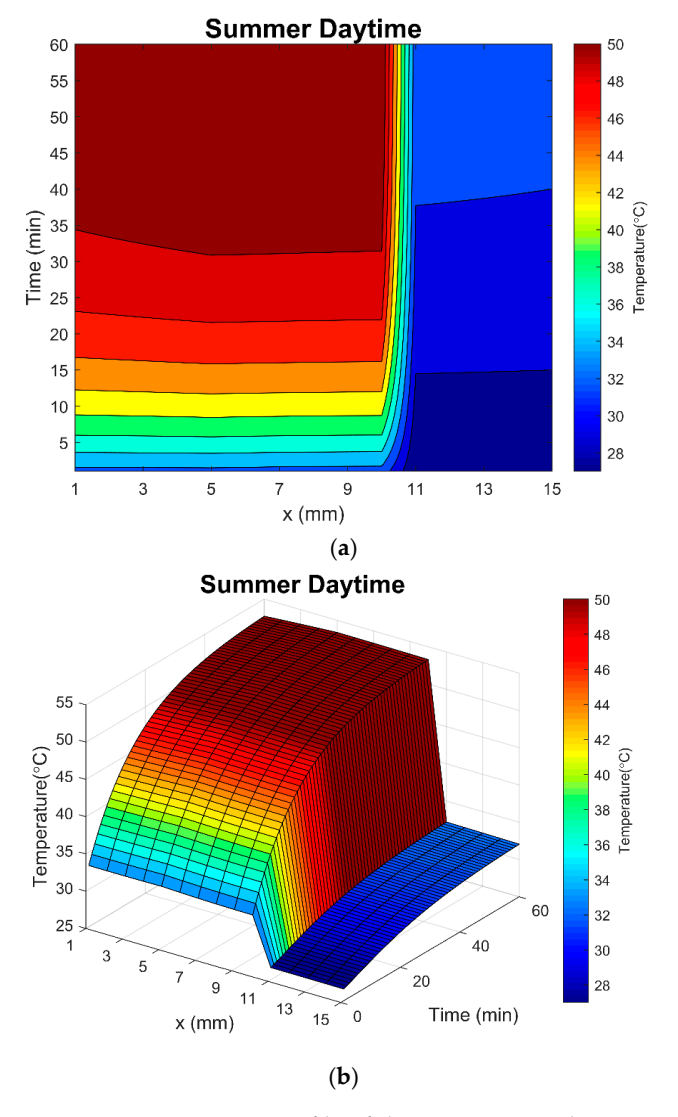


Figure 8. Temperature profile of the vacuum PV glazing under summer daytime conditions. (a) Contouring isotherms; (b) 3-D isotherms.

By the end of the simulation period, the temperatures of the exterior surface and solar cells reached 52.7 $^{\circ}$ C and 53.4 $^{\circ}$ C, increasing by 58.7% and 60.5%, respectively. In contrast, the interior surface temperature increases only by 20.6%, from 26.6 $^{\circ}$ C to 32.0 $^{\circ}$ C.

The vacuum gap significantly reduces the heat transfer through the vacuum glazing. Meanwhile, only a small amount of solar radiation reaches the back glass of the vacuum glazing ($10 < x \le 15$), as most solar energy is absorbed by the solar cells. Consequently, a larger temperature difference occurs between the front and back glass of the vacuum glazing. However, the temperature difference between the interior surface and indoor air remains quite small.

To assess the time consumed to reach the steady state, the time constant is defined as follows:

 $TC(x,t) = \frac{T(x,t) - T(x,0)}{T(x,\infty) - T(x,0)}$ (37)

where TC(x,t) and T(x,t) are the time constant and the node temperature at distance x and time t, respectively; T(x,0) and $T(x,\infty)$ are the initial temperature and the steady-state temperature, respectively.

When TC = 99%, the node temperature reaches a steady state. In the case of summer daytime, the outside surface and the solar cells reach the steady state at 54 min. The inside surface has a time constant of 57 min, reflecting the overall time constant of the vacuum PV glazing. This extended time constant is primarily attributed to the high thermal inertia of the system.

Figure 9 demonstrates the vacuum PV glazing's temperature profile under the summer nighttime conditions. The heat transfer process at night is only driven by the temperature difference between the outdoor and indoor environments. The temperatures of the front glass and the solar cells rise by approximately 6.6% and 8.5%, reaching 34.1 $^{\circ}$ C and 34.8 $^{\circ}$ C, respectively. The time constants of the exterior surface and the solar cells are 55 min and 42 min, respectively. Meanwhile, the interior surface temperature remains close to the indoor air temperature, which fluctuates between 26.3 $^{\circ}$ C and 26.5 $^{\circ}$ C.

Figure 10 shows the temperature histories of the vacuum PV glazing under summer conditions. The outside surface and the solar cells exhibit considerably higher temperatures in the summer daytime case compared to the summer nighttime case. The temperature increases in the summer daytime and nighttime are primarily due to the solar heat gain and the indoor–outdoor temperature difference, respectively. The results indicate that the temperatures of the front part of the vacuum PV glazing are significantly affected by the incident solar radiation. However, the vacuum gap can reduce the waste heat from the solar energy absorbed by the solar cells under summer conditions. As a result, the temperature difference of the inside surface between the two summer cases remains within 5.6 $^{\circ}$ C. Therefore, the vacuum PV glazing can effectively stabilize the interior surface temperature.

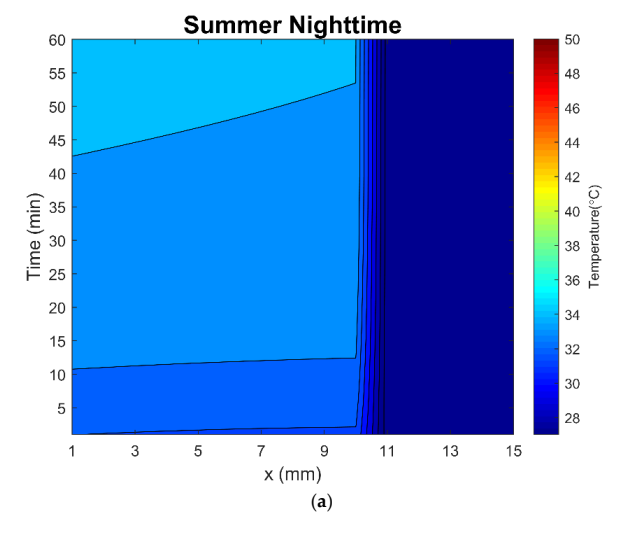


Figure 9. Cont.

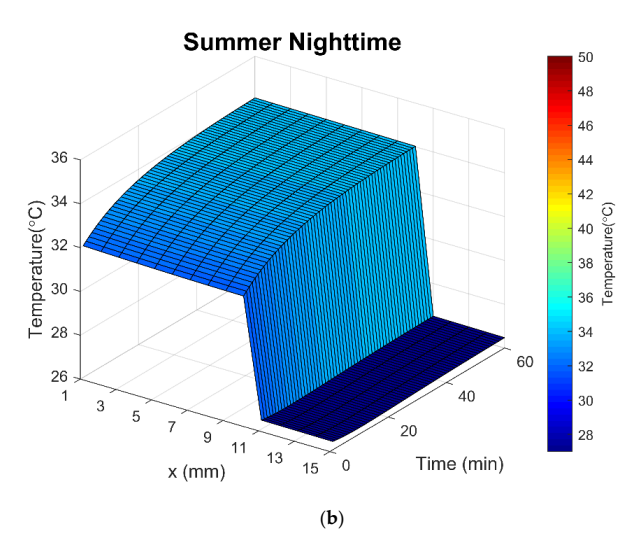


Figure 9. Temperature profile of the vacuum PV glazing under summer nighttime conditions. (a) Contouring isotherms; (b) 3-D isotherms.

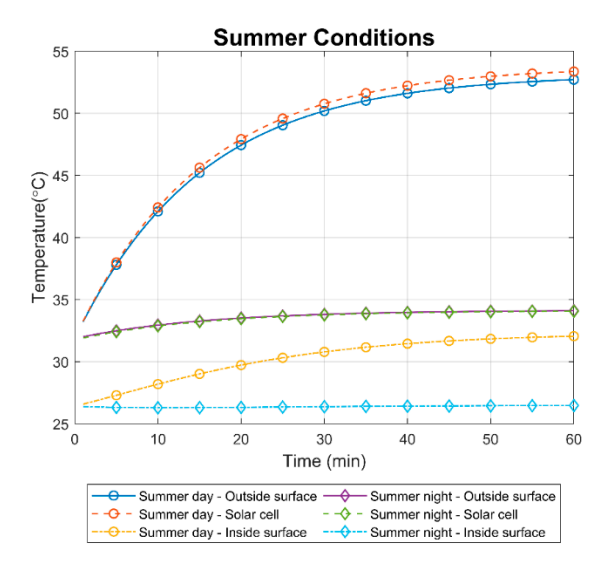


Figure 10. Surface temperature histories of the vacuum PV glazing under summer conditions.

4.1.2. Winter Conditions

For the winter cases, the outdoor air temperature is set at $-20\,^{\circ}$ C, representing a severe cold climate. During winter daytime, when the space heating is in operation, the outdoor temperature is significantly lower than the indoor temperature. Consequently, the heat loss through the window is primarily driven by the indoor–outdoor temperature difference, while solar heat gain depends on the intensity of the incident solar radiation.

Figure 11 demonstrates the contouring and the 3-D isotherms of the vacuum PV glazing under winter daytime conditions. Despite significant solar energy absorption by the solar cells, their temperature decreases from $-7.4\,^{\circ}\text{C}$ to $-11.8\,^{\circ}\text{C}$. The outside temperature, which is higher than that of the solar cells, reduces from $-8.1\,^{\circ}\text{C}$ to $-12.3\,^{\circ}\text{C}$. The temperature declines are 51.9% and 60.0% for the outside surface and solar cells, respectively. The results reveal that the heat losses, driven by the extremely low outdoor temperature, dominate the net heat flow through the front part of the vacuum PV glazing. In contrast, the insider surface temperature rises gradually by 18.0%, from 14.6 °C to 17.3 °C. The main reason is that the vacuum gap minimises the heat transfer from the indoor to the outdoor environment. In addition, the solar radiation absorbed by the back glass increases the internal energy of the substance. The time constants for the exterior and the interior surface are 44 min and 42 min, respectively.

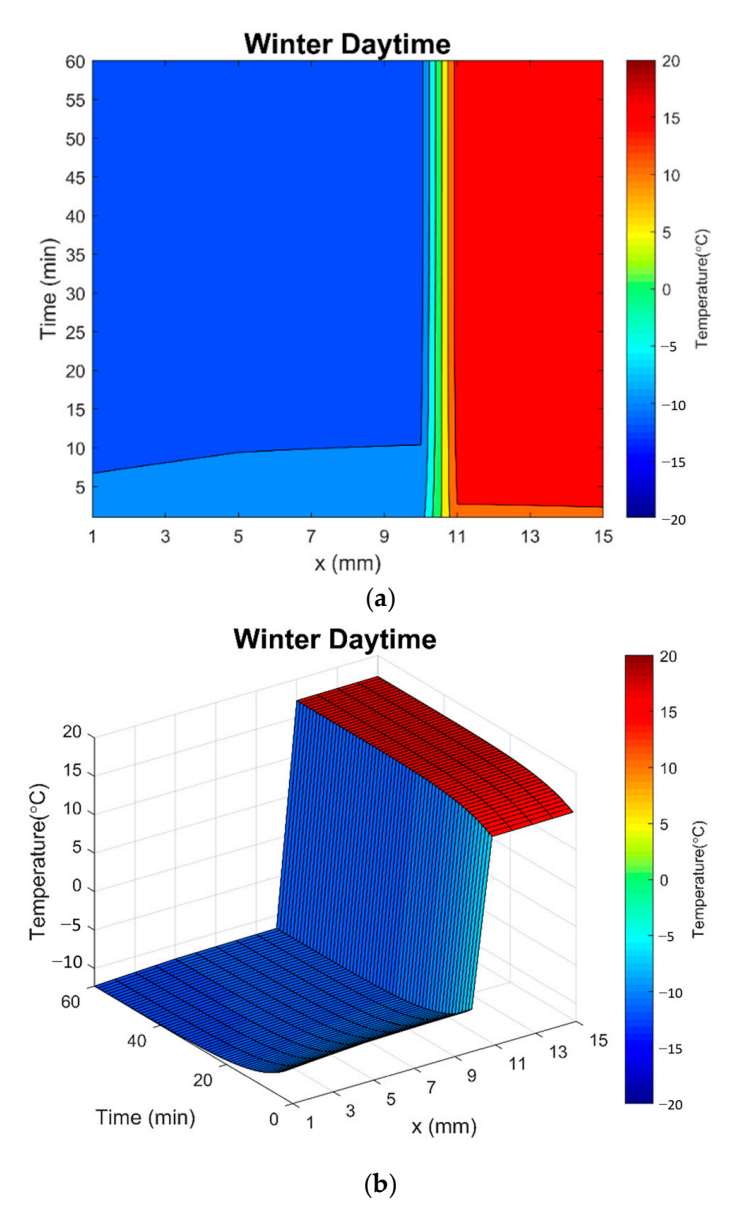


Figure 11. Temperature profile of the vacuum PV glazing under winter daytime conditions. (a) Contouring isotherms; (b) 3-D isotherms.

As demonstrated in Figure 12, the temperature profile of the vacuum PV glazing under the winter nighttime conditions closely resembles that of the winter daytime. The heat loss through the glazing is driven by the huge temperature difference between the indoor and outdoor environments. In the absence of solar radiation, the exterior surface temperature drops sharply to $-18.4~^{\circ}$ C. Meanwhile, the inside surface temperature rises slightly from 14.6 $^{\circ}$ C to 15.6 $^{\circ}$ C due to the heat exchange with the indoor air. The outside and inside surfaces reach the steady-state conditions after 45 min and 13 min, respectively. While the exterior surface temperature decreases to the outdoor temperature of $-20~^{\circ}$ C, the interior surface temperature stabilizes around the indoor temperature. The results indicate that the vacuum PV glazing minimizes the heat loss under the winter nighttime conditions.

Buildings **2025**, 15, 2612 20 of 33

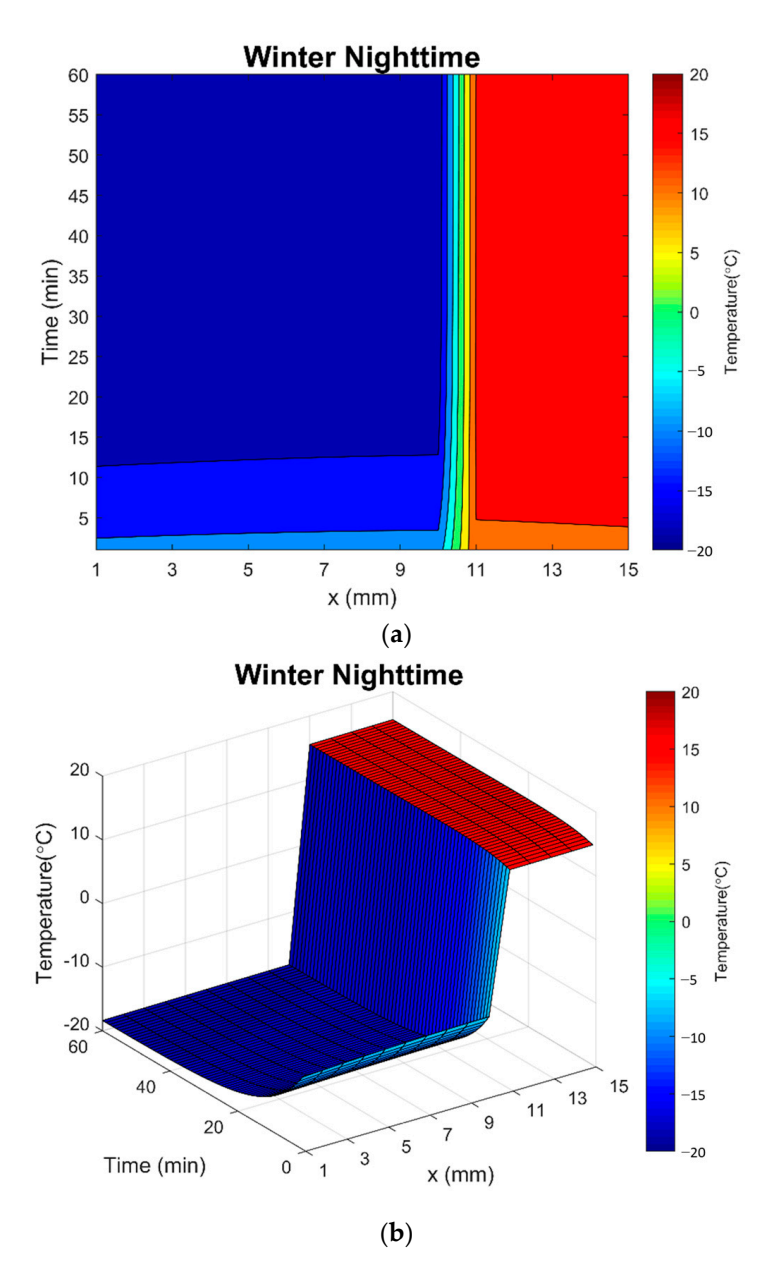


Figure 12. Temperature profile of the vacuum PV glazing under winter nighttime conditions. (a) Contouring isotherms; (b) 3-D isotherms.

Figure 13 demonstrates the temperature histories of the outside surface, solar cells, and inside surface of the vacuum PV glazing under winter conditions. The results indicate that the temperatures of these surfaces during the winter daytime are higher than those during the winter nighttime. To be specific, the temperature differences between the two cases are 6.1 °C for the outside surface, 6.4 °C for the solar cells, and 1.7 °C for the inside surface, respectively. Notably, as the temperature of the outside surface and solar cells decreases, the inside surface temperature increases. The temperature reductions in the front part of the vacuum PV glazing primarily result from heat exchange between the outside surface and the outdoor air. Similarly, the temperature increases in the back part are due to the heat exchange between the inside surface and the indoor environment. The vacuum glazing effectively isolates the heat transfer across the vacuum gap. Therefore, it can be concluded that the vacuum PV glazing shows an excellent thermal insulation performance, making it particularly suitable for regions with severely cold winters.

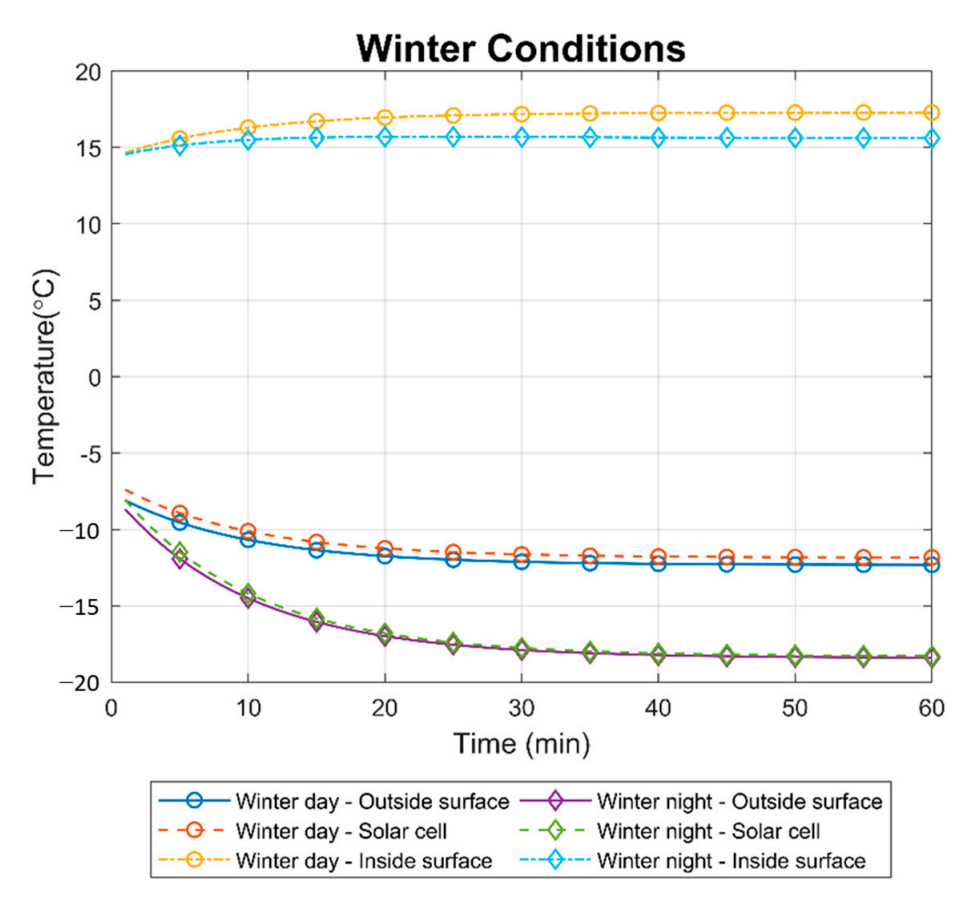


Figure 13. Surface temperature histories of the vacuum PV glazing under winter conditions.

4.2. Energy Flow Through the Vacuum PV Glazing

The vacuum PV glazing integrates the solar control ability of the PV glazing and the thermal insulation capability of the vacuum glazing. To fully understand the heat transfer mechanism of the vacuum PV glazing under different circumstances, the cases of summer daytime and winter nighttime were selected for the energy flow simulation. Based on the developed transit heat transfer model, each component of the energy flow through the vacuum PV glazing was calculated by averaging the accumulated heat gain/loss and PV power generation within 1 h.

Figure 14 shows the energy flow through the vacuum PV glazing during the summer daytime conditions. It can be seen that the solar radiation dominates the heat transfer through the glazing. The incident solar radiation partially transmits into the indoor environment since the vacuum PV glazing is semi-transparent. The remaining solar energy is absorbed by the glazing and solar cells and converted into power output and internal energy of the solid substances. Although the outdoor temperature is 10 °C higher than the indoor temperature, the convective and radiative heat on the outer surface flow outwards, which are 147.2 W/m² and 57.7 W/m², respectively. This is because the outer surface temperature is higher than the outdoor temperature due to the absorbed solar energy. For the front glass, the received solar radiation is 600 W/m², while the reflected and transmitted solar energy account for 6.75% and 78%, respectively. Since the layer of solar cells absorbed 49.1% of solar energy (294.8 W/m²), the PV cells have the highest temperature, resulting in the heat conduction to the adjacent glazing, which are 151.6 W/m² and 26.5 W/m², respectively. It also converts 41.1 W/m² of solar energy into electricity. The heat transfer between the vacuum gap consists of 112.9 W/m² of the transmitted solar radiation and 25.3 W/m² of the radiative heat. It can also be seen that the absorbed solar energy increases the internal heat of each layer to varying degrees. The total heat gain of the vacuum PV

Buildings 2025, 15, 2612 22 of 33

glazing is 107.5 W/m^2 . The direct solar transmittance is 75.1 W/m^2 , which accounts for 12.5% of incident solar energy. The secondary solar heat gain flows to the indoor environment through 23.9 W/m^2 of long-wave radiation and 8.5 W/m^2 of thermal convection, accounting for 5.4% of solar energy. In the case of a hot summer with high solar radiation intensity, the energy flow analysis demonstrates the excellent solar control ability of the vacuum PV glazing.

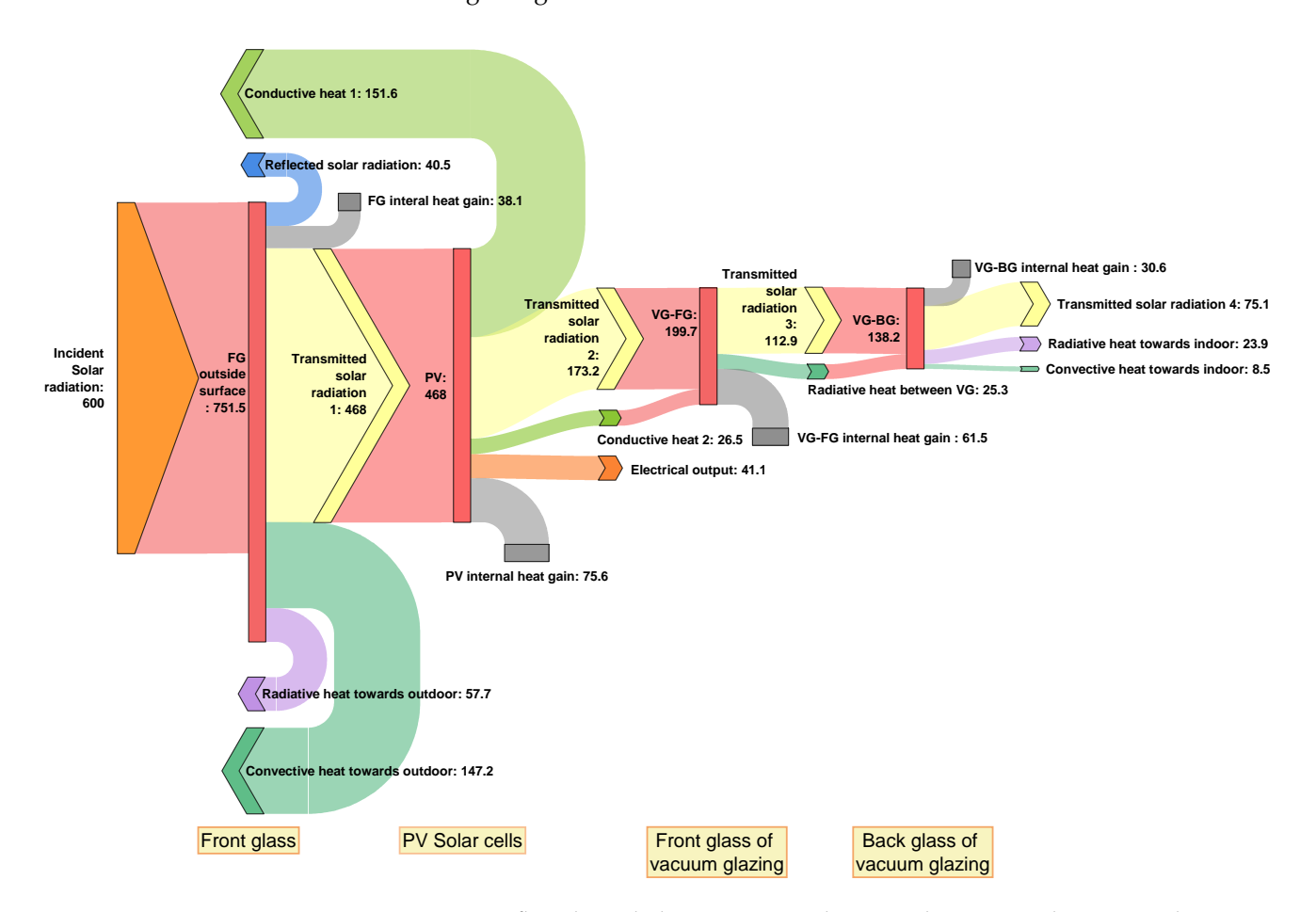


Figure 14. Energy flow through the vacuum PV glazing under summer daytime conditions.

In the winter nighttime, the temperature difference between indoors and outdoors is the only driving force for the heat transfer behaviour of the vacuum PV glazing. As shown in Figure 15, the convective and radiative heat towards outdoors are $59.7 \, \text{W/m}^2$ and $12.7 \, \text{W/m}^2$, respectively. Due to the internal heat losses of the glass panes and solar cells, the conductive heat through the front part of the vacuum PV glazing increases from $37.2 \, \text{W/m}^2$ to $51.1 \, \text{W/m}^2$. The vacuum gap minimises the heat loss from indoors to outdoors, where the radiative heat transfer between the glass sheets of the vacuum glazing is $33.6 \, \text{W/m}^2$. As a result, the internal heat of the back glass of the vacuum glazing is quite stable. The total heat loss of the vacuum PV glazing is $34.1 \, \text{W/m}^2$, including $9.8 \, \text{W/m}^2$ of heat convection and $24.3 \, \text{W/m}^2$ of heat radiation. The results indicate that the vacuum PV glazing shows an outstanding thermal insulation performance under severe cold weather conditions.

FG internal heat loss: 21.3 Radiative heat towards outdoor: 12.7 VG-FG internal heat loss: 3.7 Convective heat towards indoor: 9.8 FG Conductive VG-FG: 37.3 VG-BG: PV: 51.1 Conductive heat VG-BG internal heat gain: 0.5 PV internal heat loss: 13.9 Front glass PV solar cells Front glass of Back glass of

Energy flow through the vacuum PV glazing (W/m²)

Figure 15. Energy flow through the vacuum PV glazing under winter nighttime conditions.

vacuum glazing

4.3. Dynamic Thermal Indices

The thermal characteristics of a window system are normally determined by the overall heat transfer coefficient (U-value) and the solar heat gain coefficient (SHGC). The U-value measures how well a window conducts heat, while the SHGC measures how much solar energy passes through a window and converts it into indoor heat gain. Hence, a lower U-value indicates better thermal insulation, and a lower SHGC is an indicator of better solar control ability of a fenestration product. Typically, a static U-value and SHGC are determined under reference boundary conditions. However, due to the non-linearity of the dynamic heat transfer process, the U-value and SHGC change with the variation of local temperature. Since the local temperature depends on the absorbed solar energy and conductive heat transfer with the adjacent substances, the U-value and SHGC of the vacuum PV glazing will also change simultaneously.

Based on the transient heat transfer calculation, the dynamic U-value and SHGC of the vacuum PV glazing can be obtained under different boundary conditions to demonstrate its thermal characteristics. The calculation method of the dynamic U-value and SHGC is given by Equations (38) and (39) as follows:

$$U - value = \frac{Q_{total}(G = 0 W/m^2)}{T_o - T_{in}}$$
(38)

vacuum glazing

$$SHGC = \frac{Q_{total} - U - value(T_o - T_{in})}{G}$$
(39)

As shown in Equation (38), it is assumed that the heat transfer occurs in the absence of incoming solar radiation in the scenarios of U-value calculation. Therefore, the only driving force for heat gain or heat loss is the temperature difference between the indoor and outdoor environments. On the other hand, when there is incident solar radiation on the window, the total heat transfer is driven by both the penetration of solar heat and the temperature difference. According to ISO 15099 [41], the calculation of SHGC should

Buildings **2025**, 15, 2612 24 of 33

eliminate the influence of the indoor and outdoor temperature difference, as defined in Equation (39).

4.3.1. Dynamic U-Value

Figure 16a,b shows the dynamic U-value and total heat transfer of the vacuum PV glazing under summer and winter conditions. For the summer conditions, with the increment of temperature difference between indoors and outdoors, the heat gain increases from $0.90~\rm W/m^2$ to $5.61~\rm W/m^2$. Consequently, the dynamic U-value of the vacuum PV glazing gradually increases from $0.449~\rm W/m^2K$ to $0.467~\rm W/m^2K$. Similar changes in the heat loss and the dynamic U-value can be observed in the winter condition scenarios. As shown in Figure 16b, when the outdoor air temperature increases from $-10~\rm ^{\circ}C$ to $10~\rm ^{\circ}C$, the dynamic U-value varies from $0.414~\rm W/m^2K$ to $0.428~\rm W/m^2K$, while the heat loss decreases from $-12.43~\rm W/m^2$ to $-4.28~\rm W/m^2$. It can be found that the vacuum PV glazing has a lower U-value under the winter conditions when the heat loss occurs. In terms of the growth rate of the dynamic U-value per $1~\rm ^{\circ}C$ increment of ambient temperature, the growth rate in the summer scenarios is $0.43\%/\rm ^{\circ}C$, which is higher than the growth rate in the winter scenarios of $0.16\%/\rm ^{\circ}C$.

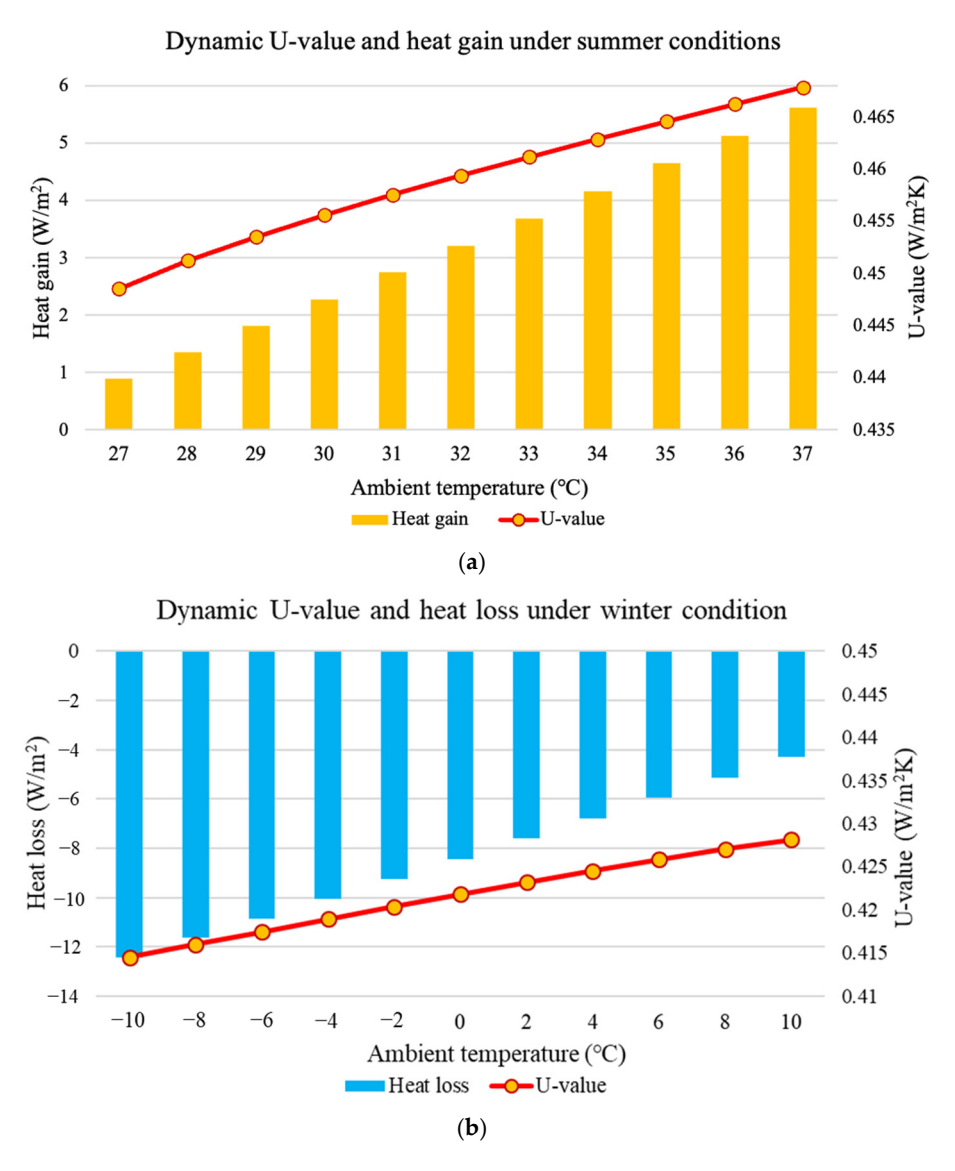


Figure 16. Cont.

Buildings **2025**, 15, 2612 25 of 33

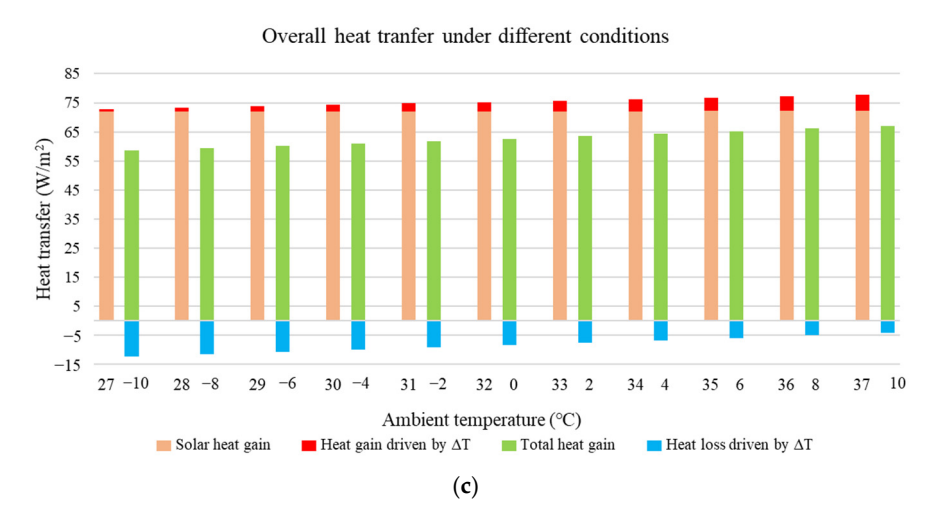


Figure 16. Dynamic U-value and heat gain of the vacuum PV glazing under summer and winter conditions. (a) Summer conditions, (b) Winter conditions, (c) Overall heat transfer.

As shown in Figure 16c, the overall heat transfer for the summer and winter scenarios is calculated with an incident solar radiation of $500~\rm W/m^2$. In the summer scenarios, the total heat gain ranges from $72.76~\rm W/m^2$ to $77.80~\rm W/m^2$. The contribution of heat transfer caused by temperature difference increases from 1.23% to 7.22%. In the winter scenarios, the overall heat transfer changes from net heat loss to net heat gain due to the incoming solar energy. As the outdoor temperature increases, the net heat gain increases from $58.5~\rm W/m^2$ to $66.9~\rm W/m^2$. For both summer and winter scenarios, the extremely low U-value of the vacuum PV glazing minimizes the heat transfer due to the indoor-outdoor temperature difference. Consequently, the solar energy transmittance dominates the overall heat transfer.

4.3.2. Dynamic SHGC

The solar heat gain of a window system consists of the direct transmitted solar energy and the secondary heat gain, where the glazing absorbs solar energy and converts it into heat convection and radiation to the indoor environment. Both the solar radiation intensity and the temperature difference between indoor and outdoor will affect the secondary heat gain. Figure 17 shows the calculation results of the dynamic SHGC of the vacuum glazing under various weather conditions. For the incident solar radiation, the input variables vary from 300 W/m² to 1000 W/m^2 . The indoor air temperature is set as $25 \,^{\circ}\text{C}$ for the summer conditions and $20 \,^{\circ}\text{C}$ for the winter conditions. The outdoor air temperatures were set to $25 \,^{\circ}\text{C}$, $30 \,^{\circ}\text{C}$, and $35 \,^{\circ}\text{C}$ for the summer scenarios 1, 2, and 3, respectively. The summer scenario 1 is considered a neutral state where the indoor and outdoor temperatures are equal. The summer scenarios 2 and 3 represent the hot and very hot levels. For the winter scenarios, the outdoor air temperature settings were $-10 \,^{\circ}\text{C}$, $0 \,^{\circ}\text{C}$, and $10 \,^{\circ}\text{C}$, to represent the cold levels as very cold, cold, and slightly cold, respectively.

As shown in Figure 17a, the dynamic SHGC of the vacuum PV glazing increases with the increment of solar radiation and outdoor air temperature. The dynamic SHGC ranges from 0.1432 to 0.1447 under different summer conditions. Comparing the highest SHGC with the lowest SHGC under different outdoor air temperature scenarios, the dynamic SHGC increases 0.52–0.64% with the increase in solar radiation. For the SHGC under the same solar radiation, the growth rate of the dynamic SHGC ranges from 0.41% ($G = 1000 \text{ W/m}^2$) to 0.53% ($G = 300 \text{ W/m}^2$) when the outdoor temperature rises. It can be seen that the dynamic SHGC is insensitive to the variations of the outdoor temperature.

Buildings **2025**, 15, 2612 26 of 33

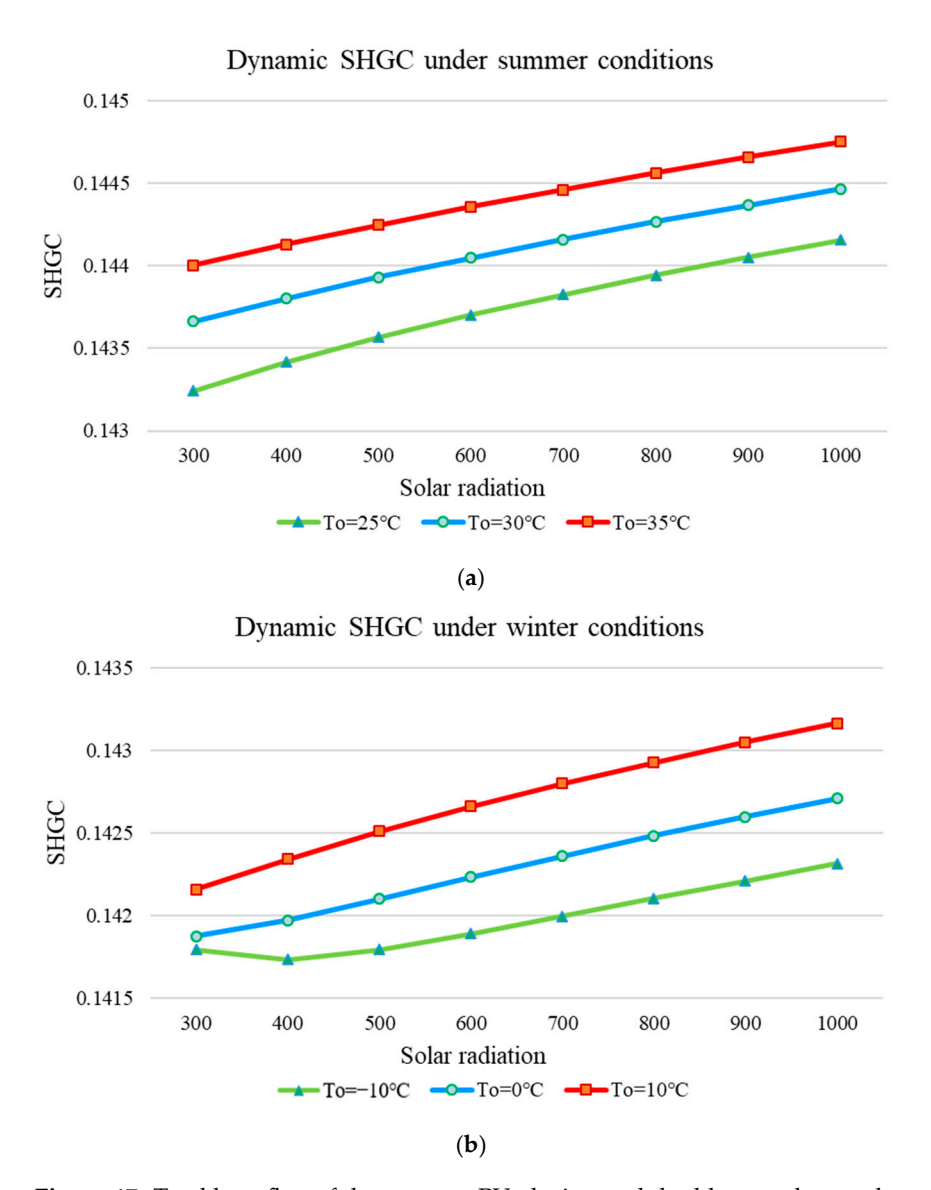


Figure 17. Total heat flux of the vacuum PV glazing and double-pane low-e glass under summer conditions. (a) Summer conditions, (b) Winter conditions.

As shown in Figure 17b, the dynamic SHGC under the winter conditions varies from 0.1417 to 0.1432, which is lower than the SHGC under the summer conditions. This is because the secondary heat gain is affected by the heat loss due to the cold environment. For the winter scenarios 1 ($T_0 = -10$ °C), 2 ($T_0 = 0$ °C) and 3 ($T_0 = 10$ °C), when the solar radiation increases from 300 W/m² to 1000 W/m², the growth rates of the dynamic SHGC are 0.37%, 0.59%, and 0.70%, respectively.

In conclusion, regarding the dynamic thermal characteristics, the CdTe-based vacuum PV glazing exhibits excellent thermal insulation and solar control capabilities under various environmental conditions. Based on the understanding of the dynamic thermal behaviours of the vacuum PV glazing as presented in Sections 4.1 and 4.2, it is known that the low U-value is mainly due to the presence of the vacuum gap, while the low SHGC is mainly due to the solar control effect of the solar cells. The thermal insulation ability also affects the SHGC of the vacuum PV glazing, resulting in the dynamic SHGC being insensitive to temperature changes. Therefore, the thermal insulation of the vacuum glazing and the solar control ability of the PV modules have a synergetic enhancement effect on the overall thermal performance of this novel BIPV glazing.

Buildings 2025, 15, 2612 27 of 33

4.4. Thermal Performance on Typical Days

To compare the thermal performance of the CdTe-based vacuum PV glazing with other common windows, the whole-day simulations were conducted based on the calculation of the dynamic heat transfer model. Four cities in China, Harbin, Beijing, Wuhan, and Guangzhou, are selected to represent different climate regions, which are known as the severe cold, cold, hot summer and cold winter, and hot summer and warm winter, respectively. The summer solstice (21 June) and the winter solstice (21 December) were chosen as the representative summer and winter days. The boundary conditions for the simulations were extracted from the weather files of the selected cities, including the indoor and outdoor temperature, incident solar radiation on the window, solar azimuth and altitude angles, and wind speed. For comparison, the hourly heat gain or heat loss of a double-pane window with low-e coating was simulated by using EnergyPlus.

Figure 18 shows the hourly heat gain or heat loss through the vacuum PV glazing and the double low-e glass under different summer conditions. Due to the difference in latitudes, the daytime of the selected cities ranges from 14 to 17 h. The peak solar radiation in Harbin and Beijing is around 300 W/m², which is higher than the peak solar radiation in Wuhan and Guangzhou of about 150 W/m². The daytime and nighttime temperature variations in Wuhan and Guangzhou are smaller than those in Beijing and Harbin. Comparing the hourly heat flux of the two glazings in different climate regions, it can be found that both heat gain and heat loss are significantly reduced by the vacuum PV glazing. In the cases of Harbin, Beijing, Wuhan, and Guangzhou, the peak heat gains of the double low-e glass are 101.2 W/m^2 , 93.4 W/m^2 , 41.2 W/m^2 , and 72.8 W/m^2 , respectively. While, in the same cases, the peak heat gain of the vacuum PV glazing is 48.4 W/m², 45.9 W/m^2 , 26.7 W/m^2 , and 26.0 W/m^2 . The maximum heat gain reduction of the vacuum PV glazing is 53.7%, 74.5%, 64.8%, and 67.3% for the cases of Harbin, Beijing, Wuhan, and Guangzhou, respectively. On the other hand, the heat loss of the vacuum PV glazing under four climate conditions is close to 0, which is much less than the heat loss of the double low-e glass during the nighttime. Therefore, compared with the double low-e glass, the application of the vacuum PV glazing will substantially reduce the cooling load during the daytime but make less use of free-cooling during the summer nights.

The winter conditions of the selected cities are quite different. Harbin and Beijing have a cold winter with the average temperature of -17.6 °C and -5.8 °C on the winter solstice, while the average temperature of Wuhan and Guangzhou is 6.5 °C and 14.0 °C, respectively. The variation in the hourly solar radiation depends on the weather conditions, such as whether it is sunny or cloudy. It can be seen that the peak incident solar radiation is higher in the winter cases than the summer cases due to the smaller solar altitude angles. As shown in Figure 19, the hourly heat flux curves of the vacuum PV glazing are much flatter than those of the double low-e glass in different climate regions. For the double low-e glass, the hourly heat flux changes sharply with the fluctuation of weather conditions. During the winter nighttime, the average heat losses through the double low-e glass are -84.3 W/m^2 , -65.7 W/m^2 , 37.0 W/m^2 , and -28.5 W/m^2 in Harbin, Beijing, Wuhan, and Guangzhou, respectively. In comparison, the average heat losses are -9.8 W/m^2 , -8.0 W/m^2 , -5.8 W/m^2 , and -4.1 W/m^2 for the vacuum PV glazing cases under the same climatic conditions. Moreover, it can be seen that the heat loss periods of the vacuum PV glazing are also shorter than those of the double low-e glass. For instance, in Harbin, at 9:00 and 15:00, the vacuum PV transfers heat gain indoors, while there are heat losses through the double low-e glass. Therefore, the vacuum PV glazing can significantly reduce the heat loss. During the daytime, the average heat gains of the vacuum PV glazing are 60.1% ~ 66.0% less than that of the double low-e glass under different climatic conditions. In terms of the total heat flux of a whole day, the vacuum

Buildings **2025**, 15, 2612 28 of 33

PV glazing performs 152.1 W/m^2 , 442.0 W/m^2 , 223.2 W/m^2 , and 605.0 W/m^2 in Harbin, Beijing, Wuhan, and Guangzhou, respectively, while the daily net heat flux of the double low-e glass are -1064.2 W/m^2 , 185.5 W/m^2 , 36.3 W/m^2 , and 1236.9 W/m^2 in the same cases. Therefore, the overall thermal performance of the vacuum PV glazing is much better than that of the double low-e glass in regions with cold winters, especially in the case of Harbin.

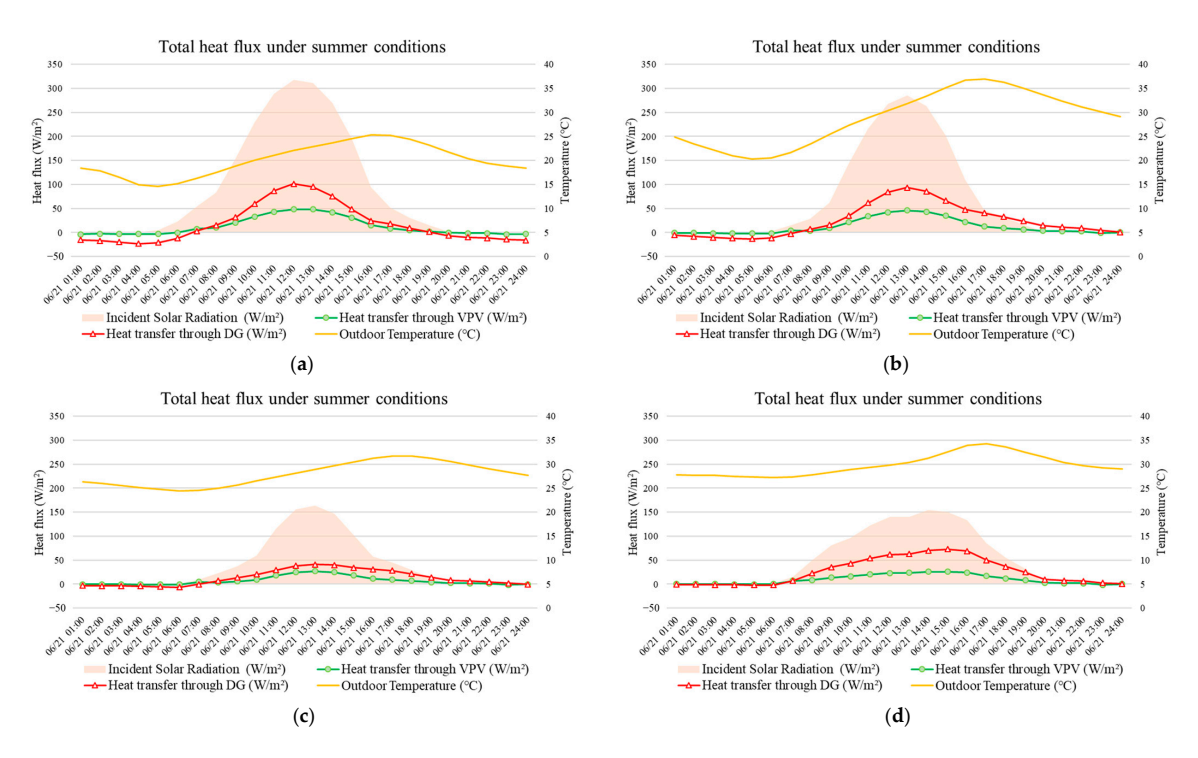


Figure 18. Hourly heat flux of the vacuum PV glazing and double-pane low-e glass on a typical summer day. (a) Harbin, (b) Beijing, (c) Wuhan, (d) Guangzhou.

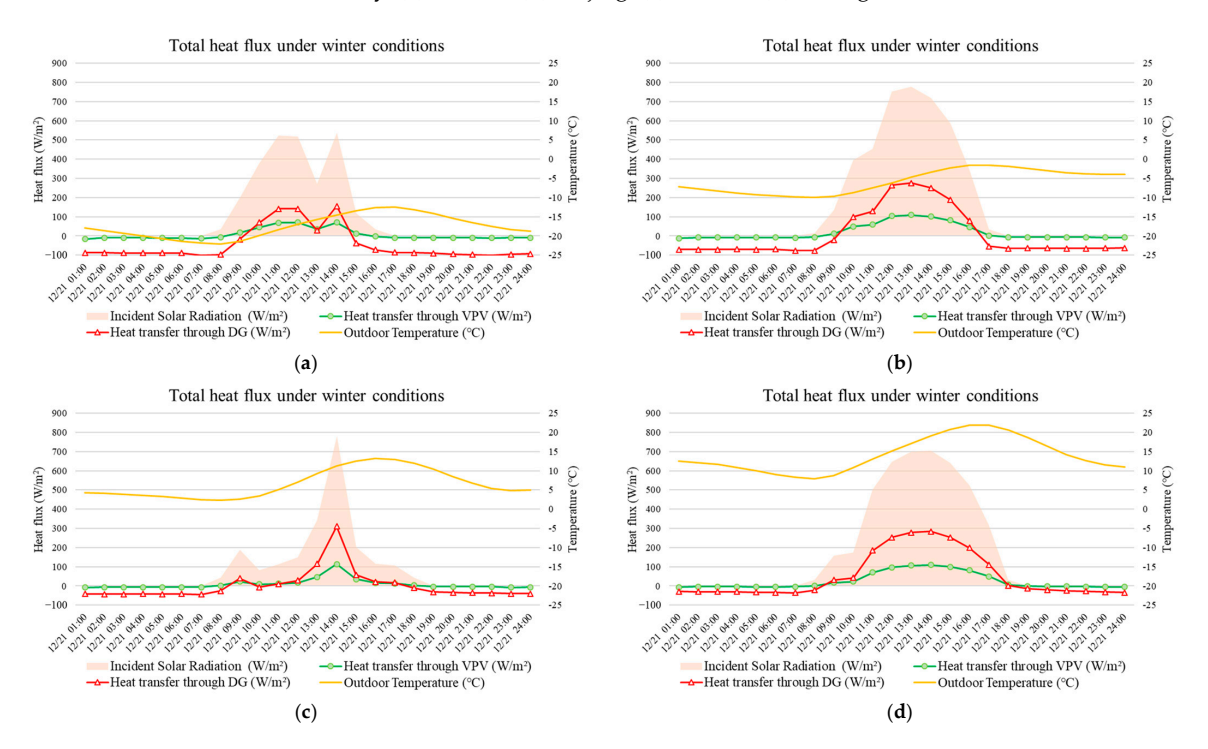


Figure 19. Hourly heat flux of the vacuum PV glazing and double-pane low-e glass on a typical winter day. (a) Harbin, (b) Beijing, (c) Wuhan, (d) Guangzhou.

Buildings 2025, 15, 2612 29 of 33

4.5. Discussion

Based on the simulation of the dynamic heat transfer process under different scenarios, the complex thermal behaviours of the CdTe-based vacuum PV glazing have been revealed from various aspects. From the analysis of temperature profile variation over time, it is worth noting that the vacuum gap acts as a thermal barrier, maintaining a stable temperature of the glass surface facing the indoor environment. Although the solar cells can absorb a large amount of heat from solar radiation, the adoption of the vacuum glazing can minimize the overheating issue caused by the waste heat transfer under summer conditions. On the other hand, in severe cold weather, despite the temperature of the outside layers decreasing rapidly, the inside surface temperature of the vacuum PV glazing tends to approach the indoor air temperature. The energy flow analysis also indicates that the vacuum PV can effectively reduce the secondary solar heat gain driven by solar radiation, as well as the heat gain or heat loss driven by temperature differences. Therefore, the vacuum PV glazing performs a superior solar control ability than conventional static glazing, such as single glass, double glass, and low-e glazing. It also shows better thermal insulation performance compared to traditional STPV windows. By applying the dynamic heat transfer modelling under real-world conditions, it can be found that vacuum PV glazing has an excellent thermal performance on both hot summer days and cold winter days. Therefore, the climate adaptability can be enhanced by combining the STPV glazing and vacuum glazing as an advanced window system.

Regarding the effectiveness of the heat transfer model, the developed dynamic heat transfer model of the CdTe-based vacuum PV glazing can determine the temperature variation with a high time-dependent resolution and fast calculation. Furthermore, the energy flow analysis can be conducted, taking into account the thermal inertia of each component. In contrast to steady-state models, which are typically used to determine the thermal properties under standard test conditions, the transient heat transfer model can be deployed under dynamic boundary conditions. Hence, it can predict the dynamic heat transfer under real-world scenarios. Moreover, since the PV power generation is sensitive to the temperature of solar cells, it is essential to obtain the time-varying temperature using the transient heat transfer modelling. Compared with 2D or 3D models, the 1D transient heat transfer model has the advantage of less computational time, which provides the opportunity for fast deployment in whole-building energy simulations.

5. Conclusions

In this study, the dynamic thermal behaviours of the CdTe-based vacuum PV glazing were studied based on the developed transit heat transfer model. The thermal performance evaluation was conducted under typical summer and winter conditions. The main findings are summarised as follows:

- 1. In summer daytime, the layer of solar cells can be recognised as a heat blocker to prevent thermal transmission due to the temperature difference between indoor and outdoor spaces. The temperature of the inside surface only has 20.6% growth, while the temperature of the outside surface and the solar cells increase by 58.7% and 60.5%, respectively. In summer nighttime, there is a larger temperature difference between the front glass of the vacuum glazing and the back glass of the vacuum glazing. However, the temperature difference between the inside surface and the indoor air is quite small. Therefore, the vacuum PV glazing enhances the stabilisation of the interior surface temperature of the PV glazing.
- 2. For the case of winter daytime, the declines in the outside surface temperature and solar cells' temperature are 51.9% and 60.0%, respectively. On the contrary, the inside surface temperature gradually increases by 18.0%. The results indicate that the solar

Buildings 2025, 15, 2612 30 of 33

radiation absorbed by the back glass of the vacuum glazing increases the internal energy of the substance. For the case of winter nighttime, the temperature of the outside surface dramatically decreases to $-18.4\,^{\circ}$ C. The inside surface temperature increases from 14.6 $^{\circ}$ C to 17.3 $^{\circ}$ C. The vacuum glazing isolates the heat transfer along both sides of the vacuum gap. In conclusion, the vacuum PV glazing is suitable for severe cold winter regions.

- 3. The heat gain of the vacuum PV glazing under the summer daytime conditions is primarily due to the incoming solar radiation. Only a small proportion of solar energy, about 12.5%, penetrates the indoor environment. Meanwhile, the secondary solar heat gain is only 32.4 W/m². The results indicate that the vacuum gap mitigates the absorbed solar energy from transferring indoors as waste heat under summer conditions. In the winter nighttime, the heat losses dominate the net heat flow through the vacuum PV glazing. The vacuum gap reduces heat transfer from indoors to outdoors. The total heat loss is 34.1 W/m², while the internal heat of the back glass is stable. Therefore, the vacuum PV glazing not only demonstrates an excellent solar control ability but also has a superior thermal insulation performance from a hot and sunny day to a severe cold night.
- 4. The dynamic U-value and SHGC of the vacuum PV glazing are much lower than other common fenestration products. Depending on the weather conditions, the dynamic U-value ranges from 0.414 W/m²K to 0.467 W/m²K. The dynamic SHGC varies from 0.1417 to 0.1447. Due to the extremely low U-value, the solar heat gain normally dominates the overall heat transfer regardless of when the incident solar radiation occurs. It is also found that there is a synergetic enhancement effect of the thermal insulation of the vacuum glazing and the solar control ability of the PV solar cells.
- 5. The net heat flux of the vacuum PV glazing is quite stabilised for the whole-day simulations under summer conditions and winter conditions. On a typical summer day, compared with the double low-e glass, the maximum heat gain reduction of the vacuum PV glazing is 53.7%, 74.5%, 64.8%, and 67.3% for the cases of Harbin, Beijing, Wuhan, and Guangzhou, respectively. On a typical winter day, the average heat losses of the vacuum PV glazing only account for 11.6%~15.7% of the average heat losses of the double low-e glass. Therefore, the vacuum PV glazing can save a large amount of cooling energy in the summer daytime and significantly reduce heating consumption for most of the day in winter.

This study extends the understanding of the heat transfer mechanism and dynamic thermal behaviour of the vacuum PV glazing. It was found that the fluctuation of the inner surface temperature can be controlled within a limited range away from the set point of the indoor room temperature. Therefore, the vacuum PV glazing is beneficial to stabilise the temperature of the controlled room despite the incident solar radiation and the periodic outdoor temperature. It is suggested that the vacuum PV glazing has the potential to enhance the thermal performance of BIPV windows under different climate backgrounds. In practical applications, the vacuum PV glazing not only produces renewable energy on-site but also enhances the climate adaptability of the building envelope due to its excellent thermal insulation and solar control ability. Furthermore, the stable inner surface temperature of the vacuum PV glazing is also beneficial for resisting condensation in humid environments. Therefore, the vacuum PV glazing application contributes to achieving energy-efficient and sustainable buildings and comfortable and healthy indoor environments.

There are also a few limitations of the current work. Since 2D or 3D simulations have the advantage of capturing more complex geometries and the heat transfer processes, it would be beneficial to expand the 1D model to high-dimensional models to study the heat

Buildings **2025**, 15, 2612 31 of 33

transfer through the vacuum PV glazing with the consideration of sealing edges. The model validation can also be enhanced via a field-based experiment under real-world conditions. In future work, to further improve the modelling complexity and reliability for practical applications, 2D or 3D modelling can be developed, taking into account the dynamic heat transfer through sealing edges and support pillars. A field experiment can be conducted to validate the model under uncontrolled environmental conditions. Furthermore, based on the dynamic heat transfer simulation, the applicability of the vacuum PV glazing can be further studied by investigating the thermal and energy performance of different types and structural configurations. For further improvement of the overall energy performance, the transient heat transfer model can be integrated with the optimization approach to optimize the structural design and key design parameters of the CdTe-based vacuum PV glazing for different climate regions.

Author Contributions: Conceptualization, H.Y.; Methodology, C.Q.; Validation, C.Q.; Investigation, C.Q.; Resources, H.Y.; Data curation, K.D.; Writing—original draft, C.Q.; Writing—review & editing, H.Y.; Supervision, H.Y. and K.D.; Funding acquisition, C.Q. All authors have read and agreed to the published version of the manuscript.

Funding: The work described in this paper was supported by the National Natural Science Foundation of China (No. 52408139), the China Postdoctoral Science Foundation Funded Project (No. 2023M743508) and the Guangzhou Science and Technology Project (2025B01J0003).

Data Availability Statement: The original contributions presented in this study are included in the article. Further inquiries can be directed to the corresponding author.

Conflicts of Interest: The authors declare no conflict of interest.

Nomenclature

Abbreviations		Greek letters		
a-Si	amorphous silicon	α	absorbance	
BAPV	building attached photovoltaics	β	temperature coefficient of solar cell	
BIPV	building integrated photovoltaic	ε	emissivity	
CdTe	cadmium telluride	η	efficiency of solar cell	
CvRMSE	coefficient of variation of root mean square error	θ_1	angle of incidence	
MBE	mean bias error	θ_2	angle of refraction	
PV	photovoltaic	λ	thermal conductivity, W/(mK)	
SHGC	solar heat gain coefficient	ρ	density, kg/m³	
STPV	semi-transparent photovoltaic	σ	Stefan–Boltzman constant, $W/(m^2K^4)$	
U-value	overall heat transfer coefficient	τ	transmittance	
Variables		Subscripts		
A_g	total area of glazing, m ²	bvg	back glass of vacuum glazing	
A_{pv}	area of solar cell, m ²	dif	diffuse solar radiation	
A_r	area of glazing without solar cell, m ²	dir	direct solar radiation	
Bi	Biot number	fg	front glass of vacuum PV glazing	
C_p	specific heat capacity, J/(kgK)	fvg	front glass of vacuum glazing	
Fo	Fourier number	i	node number	
G	incident solar radiation, W/m ²	in	indoor	
h_i	convective heat transfer coefficient on inside glazing surface, $W/(m^2K)$	o	outdoor	
h _o	convective heat transfer coefficient on outside glazing surface, $W/(m^2K)$	pv	photovoltaic solar cell	

Buildings **2025**, 15, 2612 32 of 33

I_{dif}	diffuse solar radiation, W/m ²	STC	standard test conditions
I_{dir}	direct solar radiation, W/m ²		
L	thickness, m	Superscripts	
n_1	refractive index of air	k	time step
n_2	refractive index of glass		
Q_c	convective heat flux, W/m ²		
Q_r	radiative heat flux, W/m^2		
Q_s	transmitted solar radiation, W/m^2		
Q_{total}	Total heat gain of window		
S	extinction coefficient of glass, m ⁻¹		
T	temperature, K		
t	time, s		

References

X

coordinate, m

- 1. Allen, M.; Dube, O.P.; Solecki, W.; Aragón-Durand, F.; Cramer, W.; Humphreys, S.; Kainuma, M. Special report: Global warming of 1.5 C. *Intergov. Panel Clim. Change (IPCC)* **2018**, 677, 393.
- 2. Copernicus, C. Copernicus Climate Change Service. 2024. Available online: https://climate.copernicus.eu/copernicus-2024-first-year-exceed-15degc-above-pre-industrial-level (accessed on 10 January 2025).
- 3. Giardino, A.; Pelli, M.; Raitzer, D.A.; Bosello, F.; Campagnolo, L.; Mansi, G. *Asia-Pacific Climate Report* 2024; Asian Development Bank: Mandaluyong, Philippines, 2024.
- 4. Zhang, Y.; He, C.-Q.; Tang, B.-J.; Wei, Y.-M. China's energy consumption in the building sector: A life cycle approach. *Energy Build.* **2015**, 94, 240–251. [CrossRef]
- 5. Xia, Y.; Yang, Z.; Jiang, X.; Wang, H. The road to carbon neutrality in China's building sector. *iScience* **2024**, 27, 110664. [CrossRef] [PubMed]
- 6. Mohammad, A.K.; Garrod, A.; Ghosh, A. Do Building Integrated Photovoltaic (BIPV) windows propose a promising solution for the transition toward zero energy buildings? A review. *J. Build. Eng.* **2023**, *79*, 107950. [CrossRef]
- 7. Ghosh, A. Potential of building integrated and attached/applied photovoltaic (BIPV/BAPV) for adaptive less energy-hungry building's skin: A comprehensive review. *J. Clean. Prod.* **2020**, *276*, 123343. [CrossRef]
- 8. Kosorić, V.; Lau, S.-K.; Tablada, A.; Lau, S.S.-Y. General model of Photovoltaic (PV) integration into existing public high-rise residential buildings in Singapore—Challenges and benefits. *Renew. Sustain. Energy Rev.* **2018**, *91*, 70–89. [CrossRef]
- 9. Li, Y.; Mao, Y.; Wang, W.; Wu, N. Net-Zero Energy Consumption Building in China: An Overview of Building-Integrated Photovoltaic Case and Initiative toward Sustainable Future Development. *Buildings* **2023**, *13*, 2024. [CrossRef]
- 10. Yang, S.; Fiorito, F.; Sproul, A.; Prasad, D. Optimising Design Parameters of a Building-Integrated Photovoltaic Double-Skin Facade in Different Climate Zones in Australia. *Buildings* **2023**, *13*, 1096. [CrossRef]
- 11. Liu, D.; Sun, Y.; Wilson, R.; Wu, Y. Comprehensive evaluation of window-integrated semi-transparent PV for building daylight performance. *Renew. Energy* **2020**, *145*, 1399–1411. [CrossRef]
- 12. Yu, G.; Yang, H.; Luo, D.; Cheng, X.; Ansah, M.K. A review on developments and researches of building integrated photovoltaic (BIPV) windows and shading blinds. *Renew. Sustain. Energy Rev.* **2021**, *149*, 111355. [CrossRef]
- 13. Skandalos, N.; Karamanis, D. Investigation of thermal performance of semi-transparent PV technologies. *Energy Build.* **2016**, 124, 19–34. [CrossRef]
- 14. Peng, J.; Curcija, D.C.; Lu, L.; Selkowitz, S.E.; Yang, H.; Zhang, W. Numerical investigation of the energy saving potential of a semi-transparent photovoltaic double-skin facade in a cool-summer Mediterranean climate. *Appl. Energy* **2016**, *165*, 345–356. [CrossRef]
- 15. Peng, J.; Curcija, D.C.; Thanachareonkit, A.; Lee, E.S.; Goudey, H.; Selkowitz, S.E. Study on the overall energy performance of a novel c-Si based semitransparent solar photovoltaic window. *Appl. Energy* **2019**, 242, 854–872. [CrossRef]
- Alrashidi, H.; Ghosh, A.; Issa, W.; Sellami, N.; Mallick, T.K.; Sundaram, S. Thermal performance of semitransparent CdTe BIPV window at temperate climate. Sol. Energy 2020, 195, 536–543. [CrossRef]
- 17. Qiu, C.; Yang, H.; Zhang, W. Investigation on the energy performance of a novel semi-transparent BIPV system integrated with vacuum glazing. *Build. Simul.* **2019**, *12*, 29–39. [CrossRef]
- 18. Zhang, W.; Lu, L.; Chen, X. Performance evaluation of vacuum photovoltaic insulation glass unit. In Proceedings of the 8th International Conference on Applied Energy, Beijing, China, 8–11 October 2016.

Buildings **2025**, 15, 2612 33 of 33

19. Qiu, C.; Yang, H. Daylighting and overall energy performance of a novel semi-transparent photovoltaic vacuum glazing in different climate zones. *Appl. Energy* **2020**, *276*, 115414. [CrossRef]

- 20. Qiu, C.; Yi, Y.K.; Wang, M.; Yang, H. Coupling an artificial neuron network daylighting model and building energy simulation for vacuum photovoltaic glazing. *Appl. Energy* **2020**, *263*, 114624. [CrossRef]
- 21. Huang, J.; Wang, Q.; Chen, X.; Xu, S.; Yang, H. Experimental investigation and annual overall performance comparison of different photovoltaic vacuum glazings. *Sustain. Cities Soc.* **2021**, 75, 103282. [CrossRef]
- 22. Huang, J.; Chen, X.; Peng, J.; Yang, H. Modelling analyses of the thermal property and heat transfer performance of a novel compositive PV vacuum glazing. *Renew. Energy* **2021**, *163*, 1238–1252. [CrossRef]
- 23. Uddin, M.M.; Wang, C.; Zhang, C.; Ji, J. Investigating the energy-saving performance of a CdTe-based semi-transparent photovoltaic combined hybrid vacuum glazing window system. *Energy* **2022**, *253*, 124019. [CrossRef]
- 24. Ghosh, A.; Sundaram, S.; Mallick, T.K. Investigation of thermal and electrical performances of a combined semi-transparent PV-vacuum glazing. *Appl. Energy* **2018**, 228, 1591–1600. [CrossRef]
- 25. Ghosh, A.; Sarmah, N.; Sundaram, S.; Mallick, T.K. Numerical studies of thermal comfort for semi-transparent building integrated photovoltaic (BIPV)-vacuum glazing system. *Sol. Energy* **2019**, *190*, 608–616. [CrossRef]
- 26. Jarimi, H.; Lv, Q.; Ramadan, O.; Zhang, S.; Riffat, S. Design, mathematical modelling and experimental investigation of vacuum insulated semi-transparent thin-film photovoltaic (PV) glazing. *J. Build. Eng.* **2020**, *31*, 101430. [CrossRef]
- 27. Zhang, C.; Ji, J.; Wang, C.; Ke, W.; Xie, H.; Yu, B. Experimental and numerical studies on the thermal and electrical performance of a CdTe ventilated window integrated with vacuum glazing. *Energy* **2022**, 244, 123128. [CrossRef]
- 28. Chen, B.; Lv, H.; Liao, J.; Dong, S.; Cheng, C.; Lv, Q.; Li, J.; Su, Y.; Riffat, S. Thermal insulation performance of an advanced photovoltaic vacuum glazing: A numerical investigation and simulation. *J. Renew. Sustain. Energy* **2019**, *11*, 015101. [CrossRef]
- 29. Tan, Y.; Peng, J.; Luo, Y.; Luo, Z.; Curcija, C.; Fang, Y. Numerical heat transfer modeling and climate adaptation analysis of vacuum-photovoltaic glazing. *Appl. Energy* **2022**, *312*, 118747. [CrossRef]
- 30. Radwan, A.; Katsura, T.; Memon, S.; Serageldin, A.A.; Nakamura, M.; Nagano, K. Thermal and electrical performances of semi-transparent photovoltaic glazing integrated with translucent vacuum insulation panel and vacuum glazing. *Energy Convers. Manag.* 2020, 215, 112920. [CrossRef]
- 31. Wong, P.W.; Shimoda, Y.; Nonaka, M.; Inoue, M.; Mizuno, M. Semi-transparent PV: Thermal performance, power generation, daylight modelling and energy saving potential in a residential application. *Renew. Energy* **2008**, *33*, 1024–1036. [CrossRef]
- 32. Chow, T.T.; Fong, K.F.; He, W.; Lin, Z.; Chan, A.L.S. Performance evaluation of a PV ventilated window applying to office building of Hong Kong. *Energy Build.* **2007**, *39*, 643–650. [CrossRef]
- 33. Ding, H.; Yu, G. Development of a simplified resistance-capacity network thermal model for semi-transparent photovoltaic insulating glass unit. *Sol. Energy* **2022**, 245, 165–182. [CrossRef]
- 34. Infield, D.; Eicker, U.; Fux, V.; Mei, L.; Schumacher, J. A simplified approach to thermal performance calculation for building integrated mechanically ventilated PV facades. *Build. Environ.* **2006**, *41*, 893–901. [CrossRef]
- 35. Wang, C.; Ji, J.; Uddin, M.M.; Yu, B.; Song, Z. The study of a double-skin ventilated window integrated with CdTe cells in a rural building. *Energy* **2021**, *215*, 119043. [CrossRef]
- 36. Zhang, C.; Ji, J.; Wang, C.; Ke, W. Annual analysis and comparison of the comprehensive performance of a CdTe PV ventilated window integrated with vacuum glazing in different climate regions. *Renew. Energy* **2024**, 223, 120029. [CrossRef]
- 37. Collins, R.E.; Davis, C.A.; Dey, C.J.; Robinson, S.J.; Tang, J.Z.; Turner, G.M. Measurement of local heat flow in flat evacuated glazing. *Int. J. Heat Mass Transf.* **1993**, *36*, 2553–2563. [CrossRef]
- 38. Zhang, C.; Wang, J.; Xu, X.; Zou, F.; Yu, J. Modeling and thermal performance evaluation of a switchable triple glazing exhaust air window. *Appl. Therm. Eng.* **2016**, 92, 8–17. [CrossRef]
- Curelja, D.; Goss, W.P. New correlations for convective heat transfer coefficient on indoor fenestration surfaces-compilation of more recent work. In Proceedings of the Thermal Performance of the Exterior Envelopes of Buildings VI, Clearwater, FL, USA, 4 December 1995; pp. 567–572.
- 40. *IEC 60904-9*; Photovoltaic Devices—Part 9: Solar Simulator Performance Requirements. International Electrochemical Commission (IEC): Geneva, Switzerland, 2007.
- 41. ISO 15099; Thermal Performance of Windows, Doors and Shading Devices—Detailed Calculations. ISO: Geneva, Switzerland, 2003.

Disclaimer/Publisher's Note: The statements, opinions and data contained in all publications are solely those of the individual author(s) and contributor(s) and not of MDPI and/or the editor(s). MDPI and/or the editor(s) disclaim responsibility for any injury to people or property resulting from any ideas, methods, instructions or products referred to in the content.